HHS Public Access

Author manuscript

Nat Neurosci. Author manuscript; available in PMC 2021 February 21.

Published in final edited form as:

Nat Neurosci. 2020 August ; 23(8): 939–951. doi:10.1038/s41593-020-0664-0.

AHR is a Zika virus host factor and a candidate target for antiviral therapy

Federico Giovannoni[1,2], **Irene Bosch**[3,4], **Carolina Manganeli Polonio**[5,6], **María F. Torti**[2], **Michael A. Wheeler**[1], **Zhaorong Li**[1], **Leonardo Romorini**[7], **María S. Rodriguez Varela**[7], **Veit Rothhammer**[1], **Andreia Barroso**[1], **Emily C. Tjon**[1], **Liliana M. Sanmarco**[1], **Maisa C. Takenaka**[1], **Sadeq Modaresi**[1], **Cristina Gutiérrez-Vázquez**[1], **Nágela Ghabdan Zanluqui**[6,8], **Nilton Barreto dos Santos**[9], **Carolina Demarchi Munhoz**[9], **Zhongyan Wang**[10], **Elsa B. Damonte**[2], **David Sherr**[10], **Lee Gehrke**[3,11], **Jean Pierre Schatzmann Peron**[5,6,8,13,*], **Cybele C. Garcia**[2,13,*], **Francisco J. Quintana**[1,12,13,*]

[1]Ann Romney Center for Neurologic Diseases, Brigham and Women's Hospital, Harvard Medical School, Boston, MA 02115, USA

[2]Laboratorio de Estrategias Antivirales, Departamento de Química Biológica, Facultad de Ciencias Exactas y Naturales, Universidad de Buenos Aires. CONICET- Instituto de Química Biológica (IQUIBICEN), Buenos Aires, Argentina

[3]Institute for Medical Engineering and Science, Massachusetts Institute of Technology, Cambridge, MA 02139, USA

[4]Department of Medicine, Mount Sinai School of Medicine, New York, NY 10029, USA

[5]Neuroimmune Interactions Laboratory, Immunology Department - ICB IV, University of São Paulo (USP), São Paulo, SP CEP 05508-900 Brazil.

[6]Scientific Platform Pasteur-USP, University of São Paulo (USP), São Paulo, SP CEP 05508-020 Brazil.

[7]Laboratorio de Investigación aplicada a Neurociencias (LIAN), Fundación para la Lucha contra las Enfermedades Neurológicas de la Infancia (FLENI), Ruta 9, Km 52.5, B1625XAF, Buenos Aires, Argentina.

[8]Immunopathology and Allergy Post Graduate Program, School of Medicine, University of São Paulo (USP), São Paulo, SP CEP 01246-903 Brazil.

[9]Department of Pharmacology, Institute of Biomedical Science, University of São Paulo, São Paulo, 05508-000, Brazil

[*]Correspondence to: Jean P. Schatzmann Peron. jeanpierre@usp.br, Cybele C. Garcia. cygarcia@qb.fcen.uba.ar, Francisco J. Quintana. fquintana@rics.bwh.harvard.edu.

Authors' contributions:

F.G, I.B., C.M.P., M.F.T., L.R., M.S.R.V., V.R., A.B., L.S., M.C.T., S.M., C.G.V., M.W., N.G.Z., N.B.S., C.D.M., Z.W. and J.P.S.P. performed *in vitro* and *in vivo* experiments, F.G., Z.L. and E.C.T. performed bioinformatics analysis, I.B, L.G., D.S., J.P.S.P., C.C.G. and F.J.Q. provided unique reagents, discussed and/or interpreted findings, F.G., C.C.G. and F.J.Q. wrote the manuscript and C.C.G. and F.J.Q. designed and supervised the study and edited the manuscript.

Competing financial interests

FJQ is a member of the Scientific Advisory Board of Kyn Therapeutics. DHS is a co-founder of and holds equity in Hercules Pharmaceuticals, The Netherlands. The other authors declare no competing interests.

[10]Dept. of Environmental Health, Boston University School of Public Health, MA, USA.

[11]Program in Virology, Division of Medical Sciences, Harvard Medical School, Boston MA 02215

[12]Broad Institute of MIT and Harvard, Cambridge, MA, USA.

[13]These authors contributed equally: Jean Pierre Schatzmann Peron, Cybele C. Garcia, Francisco J. Quintana

Abstract

Zika virus (ZIKV) is a flavivirus linked to multiple birth defects including microcephaly, known as congenital ZIKV syndrome. The identification of host factors involved in ZIKV replication may guide efficacious therapeutic interventions. In genome-wide transcriptional studies, we found that ZIKV infection triggers aryl hydrocarbon receptor (AHR) activation. Specifically, ZIKV infection induces kynurenine production, which activates AHR limiting the production of type I interferons involved in anti-viral immunity. Moreover, ZIKV-triggered AHR activation suppresses intrinsic immunity driven by the promyelocytic leukemia protein (PML), which limits ZIKV replication. AHR inhibition suppressed the replication of multiple ZIKV strains *in vitro*, and also of the related flavivirus dengue. Finally, AHR inhibition with a nanoparticle-delivered AHR antagonist or an inhibitor developed for human use limited ZIKV replication and ameliorated newborn microcephaly in a murine model. In summary, we identified AHR as a host factor for ZIKV replication, and PML as a driver of anti-ZIKV intrinsic immunity.

Introduction

Zika virus (ZIKV) is an enveloped, positive-sense single stranded RNA virus in the Flavivirus genus of the *Flaviviridae* family; this genus includes other viruses of public health concern such as dengue (DENV), yellow fever and Japanese encephalitis[1]. Human ZIKV infection was first reported in the 1950s in Africa , but less than 20 cases had been reported until 2007 when the first ZIKV outbreak in Yap, Gabon and the South Pacific occurred[2]. In 2014 the virus spread to the Americas and since then 87 countries reported the emergence of ZIKV[3]. The symptoms of ZIKV infection are generally mild and most ZIKV infected individuals do not develop disease. However, following its re-emergence in 2013, ZIKV has been linked to a congenital Zika syndrome characterized by fetal brain abnormalities[4], and also to Guillain–Barré syndrome[5]. Despite its association with these severe outcomes, no therapy is currently approved for the treatment of ZIKV or other flavivirus infection[6], highlighting the unmet clinical need for approaches to manage emerging flavivirus outbreaks.

The development of effective therapies against ZIKV requires a better understanding of virus-host interactions and anti-viral immunity. In addition to innate and adaptive immunity, cell intrinsic defense mechanisms collectively known as intrinsic immunity participate in the control of viral infections[7]. Intrinsic immunity is mediated by proteins that display antiviral activity and block viral replication at multiple levels, such as the products of 2’−5’-oligoadenylate synthetase 1b *(OAS1B)*[8], interferon stimulated exonuclease gene 20 *(ISG20)*

and promyelocytic leukemia[9] *(PML)* genes. Little is known, however, about restriction factors that limit ZIKV replication.

Here we report that ZIKV infection induces the production of Kynurenine (Kyn), which activates AHR leading to the suppression of type I interferon (IFN-I) production, NF-κB signaling and intrinsic immunity mechanisms that suppress viral replication. Conversely, *in vivo* treatment with AHR antagonists suppresses viral replication in mouse fetal tissues, reducing overall fetal malformations linked to congenital Zika syndrome. Collectively, these studies define AHR as a host-enabling factor for ZIKV replication and PML as a driver of anti-ZIKV intrinsic immunity, and identify AHR antagonists as candidate therapeutics for the management of ZIKV infection.

Results

AHR signaling is activated by ZIKV infection

The liver is a primary target of human ZIKV infection[10]. To identify molecular mechanisms associated with ZIKV replication, we analyzed by RNA-Seq mRNA expression in liver-derived human HepG2 cells infected with ZIKV. We detected 179 differentially expressed genes related to cellular processes such as protein translation, cell cycle control, energy metabolism and autophagy (Figs. 1a–c and Suppl. Table 1). These processes have been shown to be targeted by ZIKV and other flaviviruses to promote their replication[11, 12]. In addition, we detected significant effects of ZIKV infection on signaling by the transcription factor aryl hydrocarbon receptor (AHR) (Fig. 1c). Indeed, AHR was identified as a regulator of the transcriptional response of HepG2 cells to ZIKV infection (Fig. 1d and Suppl. Table 2). In validation studies on independent samples we detected increased expression of the AHR transcriptional targets *CYP1A1* and *CYP1B1* in ZIKV-infected HepG2 cells (Fig. 1e). These observations were further validated by analyzing RNA-Seq data available in public databases, which detected upregulated AHR signaling in ZIKV-infected human brain organoids[13] and also in full-term placentas from ZIKV-infected women[14] (Extended data 1a–c). Based on the potential for therapeutic modulation of AHR signaling by small molecules, and our own interest on the role of AHR in immunity, we explored the role of AHR in ZIKV replication.

AHR is a ligand-activated transcription factor whose transcriptional activity requires both AHR expression and the presence of AHR agonists[15]. Kyn is a tryptophan (Trp)-derived AHR ligand produced in the context of cancer and inflammation by the enzymes indoleamine 2,3-dioxigenase 1 and 2 (IDO1 and IDO2) and tryptophan 2,3-dioxigenase (TDO2) (Fig. 1f)[16]. We did not detect *IDO1* or *IDO2* expression in ZIKV-infected HepG2 cells. However, ZIKV infection upregulated *TDO2* expression and increased Kyn levels in culture supernatants, while it decreased the levels of Trp used as a substrate by TDO2 to generate Kyn (Figs. 1g,h).

ZIKV replicates in neural progenitor cells (NPCs)[12] as part of disease mechanisms thought to promote brain abnormalities in Zika congenital syndrome[17]. Indeed, we detected 49% of infection in human primary NPCs exposed to ZIKV (Extended data 2a). NPCs express AHR (Fig. 1i and Extended data 2b) ; the expression of *AHR*, its transcriptional target *CYP1A1*,

and *IDO1* and *TDO2* which promote the synthesis of the AHR agonist Kyn were upregulated by ZIKV infection (Fig. 1i). Of note, *AHR* mRNA expression was upregulated in ZIKV-infected NPCs but not in HepG2 cells (Figs. 1e,i), potentially reflecting intrinsic differences between these two cell types. Finally, the increase in *AHR, CYP1A1*, *IDO1* and *TDO2* expression in NPCs was dependent on the multiplicity of infection (MOI) (Fig. 1j), and it was also reflected as an increase in Kyn levels in culture supernatants (Fig. 1k). Taken together, these findings suggest that ZIKV-triggered Kyn production activates AHR.

AHR signaling boosts ZIKV replication in vitro

Based on its reported modulatory effects on the immune response and other biological processes[15, 18], we hypothesized that AHR signaling may affect ZIKV replication. To investigate the role of AHR on ZIKV infection we used the AHR antagonist CH223191 and the AHR agonist indoxyl-3-sulfate (I3S) which reaches the central nervous system (CNS) and whose production is dependent on the commensal flora[19, 20]. AHR inhibition with CH223191 reduced ZIKV replication (Puerto Rico strain, PRVABC59) by more than 50%, as determined by the quantification of HepG2 cells expressing viral antigen and by the quantification of infective virus particles released into HepG2 cell culture supernatants (Figs. 2a,b). Conversely, AHR activation with I3S increased the percentage of HepG2 cells expressing viral antigen (Fig. 2a). Of note, no cytotoxic effects were detected at the concentrations of CH223191 and I3S used to modulate viral replication, which resulted in significant AHR inhibition and activation, respectively (Extended data 3a). Moreover, in agreement with some[21] but not all[22] studies, we did not detect significant effects of CH223191 on HepG2 cell proliferation (Extended data 3b), suggesting that the decrease in virus antigen and titer induced by CH223191 treatment does not result from changes in cell proliferation.

To validate these findings, we knocked down AHR expression in HepG2 cells, detecting a reduction in ZIKV replication that resembled the effects of AHR pharmacological inhibition (Fig. 2c,d). Indeed, the knockdown of AHR led to a reduction of ZIKV yields comparable to that obtained following the knockdown of well-known pro-viral factors such as GRP78[23] (Fig. 2d). Moreover, AHR inhibition with CH223191 also decreased ZIKV replication in NPC cultures (Figs. 2e), and suppressed the replication of multiple ZIKV isolates from Argentina (INEVH116141), Brazil (BeH815744) and the reference ZIKV strain from Uganda (MR 766) (Figs. 2f–h).

To investigate whether AHR inhibition interferes with the viral entry step, we treated HepG2 cells with CH223191 at different early time points of ZIKV infection (pretreatment before viral entry, during viral adsorption and during virus internalization) and quantified ZIKV by qPCR two hours after infection. We detected no effect of CH223191 at these early timepoints in ZIKV infection as determined by qPCR, suggesting that AHR contributes to later stages of ZIKV replication (Fig. 2i). Taken together, these findings suggest that AHR activation favors the replication of ZIKV.

AHR limits IFN-I dependent and PML-driven intrinsic immunity to ZIKV

Type I interferons (IFN-I) limit ZIKV replication through interferon-stimulated genes (ISGs)[24]. The transcription factor NF-κB drives the expression of multiple antiviral genes, including IFN-I and ISGs[25]. Since AHR crosstalks with NF-κB in HepG2 cells[26], dendritic cells and CNS-resident cells[19, 20] and is also reported to control IFN-I production[27], we studied the role of AHR in the control of NF-κB and the anti-viral response during ZIKV replication. ZIKV infection of HepG2 cells triggered a non-significant but detectable increase in NF-κB activation (Fig. 3a). AHR inhibition boosted NF-κB activation, IFN-I and ISG expression in ZIKV-infected HepG2 cells, while it decreased ZIKV RNA levels (Figs. 3a,b). Similar results were observed following AHR inhibition in human NPCs infected with ZIKV (Fig. 3c).

To investigate the contribution of the suppression of IFN-I and ISG expression to the higher ZIKV replication associated with AHR signaling, we used monkey Vero cells which express AHR (Extended data 4) but do not produce IFN-I as a result of spontaneous gene deletions . We detected increased ZIKV replication in Vero cells as indicated by the expression of virus antigen in up to 90% of the cells at 48h post infection (p.i.) as compared with 16% achieved in HepG2 cells (Figs. 2a and 3d). A similar increase in ZIKV replication was detected when HepG2 cells were infected with ZIKV in the presence of drugs that block IFN-I signaling such as JAK1 inhibitor, trichostatin A and NaF (Extended Data 5, Fig. 3 e). Taken together, these findings suggest that ZIKV-triggered AHR activation suppresses NF-κB driven IFN-I-dependent responses that limit ZIKV replication.

IFN-I independent mechanisms also limit viral replication[28, 29]. Indeed, AHR inhibition reduced the infection of IFN-I-deficient Vero cells by about 30 %; this suppression of ZIKV replication was confirmed by the quantification of virus yield (Figs. 3d,f). Moreover, AHR inhibition also reduced virus replication when IFN-I signaling was suppressed with a JAK1 inhibitor in HepG2 cells (Fig. 3g). Collectively, these findings suggest that AHR also interferes with IFN-I-independent anti-viral mechanisms to promote ZIKV replication.

Treatment of ZIKV-infected HepG2 cells with the AHR-antagonist CH223919 increased the expression of PML (Figs. 3b,c), a restriction factor reported to inhibit the replication of the flavivirus DENV[9]. PML expression has been suggested to be induced by NF-κB signaling, but the mechanisms involved are still unclear[30]. Based on the ability of AHR to control the expression of target genes directly, and also indirectly through its effects on NF-κB and other transcription factors[15, 18], we investigated the regulation of PML expression by AHR.

A bioinformatic analysis identified candidate binding sites for AHR[18] and NF-κB in the *PML* promoter (Fig. 3h). Following ZIKV infection of HepG2 cells, in chromatin immunoprecipitation (ChIP) assays, we detected AHR recruitment to its responsive elements 1,3 and 4, but not to 2 (Fig. 3i). Moreover, NF-κB transactivated the *PML* promoter in reporter assays, but this transactivation was prevented by the co-expression of AHR (Fig. 3j). *PML* promoter transactivation by NF-κB, however, was rescued by treatment with the AHR antagonist CH223191 (Fig. 3j), concomitant with increased recruitment of NF-κB and decreased AHR recruitment to their respective responsive elements (Fig. 3j). These data suggest that AHR limits PML expression by suppressing NF-κB activation as reported in

dendritic cells, astrocytes and microglia[15, 18], and also, by interacting with AHR-responsive regulatory elements in the *PML* promoter.

To investigate the contribution of PML to the suppressive effects of AHR inhibition on ZIKV replication in HepG2 cells, we performed siRNA knockdown studies. The knockdown of PML expression partially abrogated the suppressive effect of CH223191 on viral replication (Fig. 3k). Conversely, the overexpression of PML isoform III, which we recently reported limits the replication of DENV[9], suppressed ZIKV replication (Fig. 3l). Collectively, these findings identify PML as a host restriction factor for ZIKV replication and suggest that AHR limits IFN-I-dependent antiviral mechanisms as well as PML-driven intrinsic immunity to ZIKV.

AHR inhibition reduces ZIKV replication in vivo and ameliorates microcephaly

ZIKV infection during pregnancy has been linked to congenital Zika syndrome, characterized by multiple birth defects including microcephaly and intra-uterine growth restriction (IUGR)[4]. ZIKV infection of pregnant mice of the SJL strain recapitulates several features of congenital Zika syndrome, such as microcephaly and cortical brain damage[17]. Based on our findings on the role of AHR as a host factor for ZIKV replication, we evaluated the therapeutic potential of AHR inhibition in pregnant SJL mice infected with ZIKV. First, we used the AHR antagonist CH223191 formulated in nanoliposomes (NLP_{ANT}) to increase its solubility and biodistribution; empty nanoliposomes (NLP) were used as controls (Fig. 4a). NLP_{ANT} inhibited AHR activation by Kyn in a luciferase reporter assay (Fig. 4b), and also suppressed the expression of the AHR-driven *Cyp1b1* gene in primary murine dendritic cells (Fig. 4c), demonstrating that NLP-formulated CH-223191 can suppress AHR signaling.

Pregnant female SJL mice were infected with 10^6 PFUs of ZIKV and treated daily with i.p. injections (5 mg/kg bodyweight, total volume 100 μl) of NLP_{ANT} or NLP. NLP_{ANT} treatment ameliorated fetal IUGR and microcephaly (Figs. 4d), while it also reduced ZIKV viral load in brain and spleen of newborn pups (Figs. 4e,f), indicating that AHR inhibition by NLP_{ANT} limits ZIKV replication *in vivo*. Moreover, NLP_{ANT} treatment reversed the reduction of biparietal length induced by ZIKV, and also showed a trend towards improvement of crown-rump and skull length which did not achieve statistical significance (Figs. 4g–k). AHR antagonism by NLP_{ANT} also diminished fetal brain pathology induced by ZIKV, as evidenced by thicker cortical plates and reduced ventricle sizes (Fig. 4l).

To further investigate the effects of AHR antagonism on ZIKV-induced defects on fetal development, we analyzed by RNA-Seq fetal mouse CNS samples. NLP_{ANT} treatment decreased the expression of AHR-driven transcriptional responses, and also of genes associated with apoptosis, tissue damage and autophagy previously linked to ZIKV-induced CNS pathology[17] (Figs. 5a–c and Suppl. Table 3). Conversely, AHR inhibition with NLP_{ANT} was associated with *Pml* upregulation and the increased expression of transcriptional programs indicative of NF-κB activation and IFN-I signaling (Figs. 5a–c). Similar results were obtained when these samples were analyzed using a PCR array, which detected the upregulation of transcriptional modules associated with NF-κB signaling and anti-microbial immunity following NLP_{ANT} administration. Taken together, these findings

suggest that AHR inhibition boosts immune mechanisms that limit ZIKV replication and pathology *in vivo* (Figs. 5d and Suppl. Table 4).

To investigate the translational relevance of AHR inhibition for the management of ZIKV infection, we evaluated a second generation non-toxic AHR antagonist (HP163) developed for the therapeutic inhibition of AHR in cancer, where AHR has been linked to tumor pathology through multiple mechanisms[31]. Of note, after oral gavage 51% of HP163 is bioavailable and 25% penetrates the blood brain barrier. HP163 suppressed basal AHR activation, as well as activation induced by Kyn, as determined in luciferase reporter assays and western blot studies in cell culture experiments (Extended data 6a–c). HP163 administration by gavage (2.5 mg/kg bodyweight in a volume of 100 μl) to pregnant SJL mice reduced fetal CNS pathology associated with ZIKV infection, as indicated by the prevention of ventricular dilation, cortical thinning and overall reduction in brain size in pups (Figs. 6a,b). Similar to results obtained with $NLP_{ANT,}$ HP163 treatment reduced fetal ZIKV viral loads in the brain, eyes and spleen, and also the viral load detected in the placenta of treated mothers (Figs. 6c–f). HP163 administration also suppressed IUGR, as indicated by the preservation of body and skull size and morphometric features (crown-rump, skull length, biparietal length and cranial height, Figs. 6g–k).

To further evaluate the effects of HP163 *in vivo*, we analyzed by immunofluorescence ZIKV and progenitor cells in the brains of infected mouse fetuses. HP163 administration decreased the number of ZIKV-infected hippocampal cells, preserving the number of nestin positive progenitor cells (Fig. 6l). In agreement with the reduction of ZIKV titers in the fetal brain, HP163 administration resulted in decreased microglial activation as indicated by reduced *Iba-11* expression (Fig. 6m). Taken together, these findings support a role for AHR signaling in ZIKV replication and pathogenesis *in vivo*, and identify AHR antagonism as candidate therapeutic approach for congenital Zika syndrome.

AHR inhibition suppresses DENV replication

PML and IFN-I limit the replication of the flavivirus DENV[9, 24]. Based on the suppression of anti-viral responses by AHR and the conservation of host factors supporting flavivirus replication, we investigated the role of AHR in DENV replication. I3S activated AHR and increased the yield of DENV in human A549 cells (Extended data 7a,b). Conversely, the AHR antagonist CH223191 inhibited the replication of the four DENV serotypes (Fig. 7a). This inhibition of DENV replication was also detected when viral RNA and viral protein expression were quantified (Figs. 7b,c). Importantly, AHR knockdown also reduced DENV yield (Figs. 7d); this inhibition was comparable to the suppression of viral production achieved by the knockdown of other targets reported to promote DENV replication such as GRP78 and HSP70[23, 32] (Fig. 7e). Taken together, these findings suggest that AHR promotes DENV replication.

Discussion

Host factors are potential therapeutic targets against multiple viral infections, including flaviviruses[33, 34]. Thus, the identification of host factors that contribute to ZIKV replication may guide the development of efficacious therapies for ZIKV infection. However, although

the oligosaccharyltransferase complex was recently reported to participate in ZIKV replication[35], little is known about additional host factors or how to target them therapeutically. Herein we report that ZIKV-triggered Kyn production results in AHR activation and the suppression of IFN-I expression (Extended data 8), suggesting that AHR is a host factor for ZIKV replication resembling previous findings made in the context of infection by other DNA and RNA viruses[27, 36].

IFN-I plays a central role in anti-viral immunity, but dysregulated IFN-I signaling may result in detrimental inflammation and immunopathology during viral infections[37]. Based on the upregulation of AHR expression by IFN-I[20], IL-6, IL-27 and other cytokines involved in antiviral immunity, these findings suggest that AHR participates in a negative feedback regulatory loop that limits immunopathology. Indeed, AHR has also been shown to restrict the potential deleterious activity of innate immune cells and effector T cells[38]. Hence, these findings suggest that ZIKV exploits AHR-driven immunoregulatory mechanisms to evade the immune response, resembling recent reports of AHR activation in the context of tumor immune evasion[39]. In addition, ZIKV infection *in vivo* may also induce the production of additional AHR agonists besides Kyn and/or suppress the degradation of natural agonists by inhibiting cytochrome P4501 (CYP1) enzymes[40] to further limit IFN-I dependent and IFN-I independent anti-viral mechanisms via AHR.

Using a murine model of ZIKV infection, we found that AHR inhibition limits viral replication, identifying AHR antagonists as candidates for antiviral therapy. Multiple models of ZIKV vertical transmission have been established using different inoculation routes such as intravenous , intra-jugular , intra-vaginal , sub-cutaneous , trans-uterine , intra-amniotic fluid and also intra-peritoneal . We recently described ZIKV vertical transmission in SJL mice following high viral inoculation (10^{10}–10^{12} PFUs) by intravenous route[17]; this experimental model also recapitulates the development of microcephaly and cortical brain damage[17]. In the studies described in this manuscript we used a 10^6 PFUs inoculum administered by the intra-peritoneal route to circumvent the need for high inoculum (10^{10}–10^{12} PFUs). Most importantly, this model uses SJL wild type mice with functional IFN-I signaling, an important point based on the effects of AHR on both IFN-I dependent and IFN-I independent anti-viral immunity.

Complex effects of interferon signaling have been described in models of ZIKV congenital syndrome. Mice lacking type I and II interferon receptors show increased susceptibility to ZIKV infection and are used as disease models to recapitulate the development of fetal brain malformations. Conversely, type I IFN (IFN-I) signaling in the fetus has been recently reported to promote pathology in an experimental model of ZIKV congenital syndrome[41]. In our studies, AHR inhibitors increased IFN-I signaling and decreased fetal pathology. Based on the anti-viral effects of IFN-I in ZIKV infection, our findings of increased IFN-I signaling concomitant with decreased viral titers and fetal pathology suggests that AHR antagonism ameliorates experimental ZIKV congenital syndrome by limiting viral replication and not through its potential effects on interferon-mediated fetal damage.

Drugs targeting host factors for antiviral therapy provide an alternative approach to classic antiviral drugs targeting viral components. Targeting host factors offers two key advantages:

(i) a broader spectrum of activity as a result of the targeting of a factor required for the replication of many viruses, and (ii) a reduced risk for selection of drug-resistant variants. However, this approach has the potential of unwanted side effects resulting from the targeting of host cellular pathways. AHR signaling plays a physiological role in pregnancy and fetal development; AHR genetic deletion or hyperactivation have been linked to fetal abnormalities[42]. Hence, AHR hyperactivation triggered by ZIKV may contribute to the pathogenesis of ZIKV congenital syndrome by directly regulating the expression of development-related genes. Moreover, these findings suggest that pharmacological AHR inhibitors may ameliorate ZIKV congenital syndrome not only as a result of their inhibitory effects on ZIKV replication, but also because of their ability to inhibit ZIKV-triggered AHR hyperactivation and its effects on developmental genes. Taken together with the reported role of AHR in the control of multiple aspects of anti-viral immunity[43–45], these findings support repurposing AHR antagonists developed for cancer immunotherapy[46] for the management of ZIKV and potentially, DENV infection. However, although the available preclinical data suggest that AHR inhibition with HP163 does not result in overt toxicity or adverse “on-target” effects, additional studies are needed to evaluate the safety of this and other AHR antagonists, particularly during pregnancy.

PML is reported to limit viral replication through multiple mechanisms including the sequestration of viral proteins, the inhibition of viral mRNA synthesis and the induction of apoptosis and autophagy in infected cells[47], but its role in ZIKV infection was previously unknown. Moreover, little is known about IFN-independent signaling pathways that control PML expression[47]. We identified PML as a factor that limits ZIKV replication and NF-κB as a driver of *PML* expression; AHR interferes with *PML* expression by limiting NF-κB activation (Extended data 8). AHR also controls phosphorylation cascades and ubiquitin-driven protein degradation , and post-translational modifications are reported to regulate PML activity[47]. Hence, it is conceivable that ZIKV-driven AHR signaling interferes with PML antiviral immunity at multiple levels. In addition, these findings suggest that the balance between NF-κB and AHR signaling regulates PML-driven intrinsic immunity to ZIKV, and potentially other viruses such as DENV[9].

Individuals within a population show heterogeneous susceptibility to viral infections and virus-induced pathology, but the mechanisms involved are poorly understood. Environmental factors such as pollutants, the diet and the microbiome affect the course and clinical outcome of infections by multiple viruses, including ZIKV[48, 49]. AHR agonists are not only produced by host metabolism, they are also provided by environmental pollutants, the diet and the commensal flora[15]. Indeed, microbial metabolites derived from dietary Trp activate AHR in astrocytes and microglia, limiting inflammation and neurodegeneration[19, 20]; microbial metabolites also activate AHR in the liver[50]. Based on the role of the CNS and the liver in ZIKV pathology and replication, our findings suggest that the modulation of AHR signaling by environmental agonists may impact multiple aspects of ZIKV infection.

In summary, we identified AHR as a ZIKV host factor, which interferes with IFN-I-driven and PML-dependent anti-viral immunity. These findings identify AHR as a candidate therapeutic target for ZIKV and, potentially, other flaviviruses. In addition, our findings

define AHR signaling as a candidate pathway by which environmental factors may influence the course of ZIKV infection and its associated pathology.

Methods

Cells, antibodies and reagents.

HepG2 (ATCC, HB-8065), A549 (ATCC® CCL-185™), HeLa (ATCC, CCL-2) and Vero cells (African green monkey kidney) (ATCC, CCL-81) were grown in Dulbecco's Modified Eagle's medium (DMEM, GIBCO) supplemented with 10 % fetal bovine serum, 100 IU/ml of penicillin and 100ug/ml of streptomycin. HEK-293 cells (ATCC, CRL-1573) and SUM149 cells (Asterand Bioscience, Detroit, MI) were grown in DMEM/F12 (GIBCO) supplemented with 10 % fetal bovine serum, 100 IU/ml of penicillin and 100ug/ml of streptomycin. C6/36 mosquito cells from *Aedes albopictus* were used to generate viral stocks, and were cultured in L-15 medium (Leibovitz) (GIBCO) supplemented with 0.3 % tryptose phosphate broth, 0.02 % glutamine, 1 % MEM non-essential amino acids solution and 10 % fetal bovine serum. NPCs(≥ 90% SOX1+/Nestin+) derived from human pluripotent stem cells (PSCs) under serum-free conditions (Stem Cell Technologies, Catalog # 70901, https://cdn.stemcell.com/media/files/pis/DX21378-PIS_1_1_0.pdf were grown using neural progenitor medium 2 (Stem Cell Technologies). Murine DCs were differentiated from bone marrow cells isolated from the femurs and tibiae of naïve B6 mice and cultured for 9 days in the presence of granulocyte macrophage colony-stimulating factor (GM-CSF, 20 ng/ml) in not treated Petri dishes. Cells were collected at day 9 and BMDCs were characterized as CD11c+MHC-II+Ly6G− cells. Murine oral cancer (MOC) 1[51] were the generous gift of Dr. R. Uppaluri.

Antibodies were used as follows: anti-flavivirus (Santa Cruz Biotechnology, 1:200 for flow cytometry), anti-AHR (Abcam ab2769, 5 μg per ChIP reaction), anti-NF-κB p65 (Cell Signaling, #D14E12, 1:1000 for WB and 5 μg per ChIP reaction), anti-GAPDH (Cell Signaling, #14C10, 1:1000 for WB), anti-phospho-NF-κB p65 (Ser536) (Cell Signaling, #93H1, 1:1000 for WB), anti-rabbit IgG HRP-linked (Cell Signaling, #7074, 1:3000 for WB).

Viral Infection.

Cells were infected at a MOI of 0.1–10. The cells were incubated for 1 h at 37 °C prior to removal of the viral inoculum and washing three times with PBS. Finally, fresh medium supplemented with 2% fetal bovine serum was added.

Plaque assay.

Vero cells were seeded into 24-well microplates and grown overnight. Ten fold dilutions of virus samples were added to monolayers of confluent Vero cells at 37°C for 1 h. Following incubation, the inoculum was removed, and monolayers overlaid with 1 ml of MEM containing 1% methylcellulose. The cells were incubated at 37 °C for 4 days and fixed using 4% formaldehyde. Finally, plaques were stained with 0.1% crystal violet in 20% ethanol and counted.

Small molecules.

I3S (Sigma, used at 50–500 μM), CH223191 (Tocris, used at 2–30 μM), Sodium fluoride (Sigma, 1 mM), Trichostatin A (Sigma, 100 nM), JAK I Inhibitor (Santa Cruz Biotechnology, 1 μM). HP163 was provided by Hercules Pharmaceuticals, BV, (Galileiweg 8, 2333 BD, The Netherlands). As tested by Pharmacelsus GmbH, a PK/PD contract research organization, the maximal plasma concentration of HP163 after i.v. administration of 5 mg/ml in mice is 4.1 ug/ml. After oral gavage, 51% of the drug is bioavailable and 25% penetrates the blood brain barrier. Dose escalation studies show no acute HP163-mediated toxicity at least up to doses of 300 mg/kg in mice and rats; no toxicity was seen in mice after daily dosing with 100 mg/kg over a six month period. HP163 is negative in the hERG (K^+ channel patch-clamp) cardiotoxicity assay. A CEREP diversity panel evaluated by Eurofins Discovery demonstrated no reactivity in 70 binding assays for G-coupled protein receptors, transporters, ion channels or nuclear receptors and in 27 enzyme assays including kinases and metabolizing enzymes.

AHR ligands and treatments.

Stock solutions of I3S, Kyn, TCDD, HP163 and CH223191 were prepared in DMSO, aliquoted and stored according to manufacturer's instructions. For CH223191, cells were pre-treated for 90 minutes and then used for further studies. For I3S, cells were pre-treated overnight.

Cell viability assay.

Cell cultures grown in 96-well plates were exposed for 48 h to serial two-fold compound dilutions, three wells for each concentration and viability was measured with 3-(4,5-dimethylthiazol-2-yl)-2,5-diphenyl tetrazolium bromide (MTT, Sigma-Aldrich).

Viral stocks.

C6/36 mosquito cells were infected at a multiplicity of infection of 1 with ZIKV Puerto Rico strain (PRVABC59); viral isolate from Argentina (INEVH116141) provided by Instituto Nacional de Enfermedades Virales Humanas, Pergamino, Argentina, ZIKV Brazil (BeH815744) gene bank accession number KU365780.1 gently provided by Prof. José Luiz Proença Modena and Daniele Durigon and reference ZIKV strain from Uganda (MR766), for 1 h at 37 °C in serum-free DMEM. DENV strains used, including DENV-1 (Hawaii), DENV-2 (New Guinea C), DENV-3 (H87) and DENV-4 (8124), were provided by Dr. A.S. Mistchenko (Hospital de Ninos Dr. Ricardo Gutierrez, Buenos Aires, Argentina). Quantification of viral titers was performed by a standard plaque assay in Vero cells.

Flow cytometry staining and acquisition.

Cells were fixed and permeabilized using Cytofix/Cytoperm (BD Biosciences). Secondary antibody for flow cytometry was phycoerythrin (PE) goat anti-mouse IgG (BD Biosciences) at a concentration of 1:200. Cells were analyzed on a Guava easyCyte flow cytometer and data was processed using FlowJo software.

qPCR.

RNA was extracted using the RNAeasy kit (Qiagen). cDNA was synthesized using the High-Capacity cDNA Reverse Transcription kit (Applied Biosystems) and qPCR was performed using TaqMan Fast Advanced Master Mix (Applied Biosystems). Gene expression was normalized to GAPDH. Primers and probes (Applied Biosystems) were: *GAPDH* Hs02786624_g1, *IFNB1* Hs01077958_s1, *AHR* Hs00169233_m1, *PML* Hs00971694_m1, *CYP1A1* Hs01054796_g1, *IFITM1* Hs00705137_s1, *CYP1B1* Hs02382916_s1, *CXCL10* Hs00171042_m1, *IDO1* Hs00984148_m1, *IDO2* Hs01589373_m1, *IFITM Hs00705137_s1*, *TDO* Hs00194611_m1. Primers and probes for the specific detection of ZIKV RNA were utilized as previously described[52, 53]. For viral load determination *in vivo*, brains and spleens from pups were macerated on trizol (Invitrogen) for RNA extraction. RNA pellets were resuspended in RNase-free water and quantified by spectrophotometry (NanoDrop, Thermo Scientific) and stored at −80 °C. Primers/probes specific for ZIKV were from Sigma Life Science and sequences ZIKV 835, ZIKV 911c and ZIKV 860-FAM were used as previously described[54]. qPCR was performed with 10 μl of each sample and 10 μl of the AgPath-IDTM One-Step RT–PCR reagents (Applied Biosystems). The amplification was performed using Quanti Studio 3 thermo cycler (Thermo Scientific). Beta-actin was used as endogenous control of the reaction. Quantification was compared with threshold cycle (Ct) value with a ZIKV plasmid standard curve.

For qPCR of Vero cells, SYBR Green PCR Master Mix (Applied Biosystems) was used. Primer pairs employed include: *ACTIN* (forward: 5'-TTAGTTGCGTTACACCCTTTCTTG-3'; reverse: 5'-TCACCTTCACCGTTCCAGTTT-3'), *AHR* (forward: 5'-ATCCTTCCAAGCGGCATAGAGACC-3'; reverse: 5'-CAAAGAAGCTCTTGGCTCTCAGG-3'), *CYP1A1* (forward: 5'-GAACTGCTTAGCCTAGTCAACCTG-3'; reverse: 5'-AGAATAGGGATGAAGTCAGCTGGG-3') and *CYP1B1* (forward: 5'-AACACCTCTGTCTTGGGCTACCAC-3'; reverse: 5'-TGGGTCATGATTCACAGACCACTGG-3')

Plasmids, transfections and luciferase assays.

PML shRNA plasmid (sc-36284-SH) was obtained from Santa Cruz Biotechnology. Transfection of HeLa cells was performed using Lipofectamine 2000 (Thermo Fisher) according to manufacturer's instructions. The plasmid encoding for the promoter region of *PML*, placed upstream of the Gaussia Luciferase (GLuc) reporter gene, was obtained from Genecopoeia. For the luciferase assay, HEK-293 cells were grown in 96 well-plates and transfected using Fugene-HD Transfection Reagent (Roche). Plasmids used for transfection in each condition are indicated in the experiment. 24 h later, pGudluc activity was analyzed using BioLux Gaussia Luciferase Assay Kit (New England Biolabs) and normalized to TK-Renilla luciferase activity, measured using the Renilla Luciferase Assay System (Promega). MOC1 and SUM149 cells were co-transfected with the pGudluc reporter plasmid (0.5 μg) (generously provided by Dr. M. Denison, UC, Davis), and CMV-green (0.1 μg) for normalization using TransIT-2020 transfection reagent (Mirus). Transfection medium was replaced after 24 hours. The cells were left untreated or dosed with vehicle (DMSO or AHR inhibitors) and harvested after 24 hours in Glo Lysis Buffer (Promega). Luciferase activity

was determined with the Bright-Glo Luciferase System according to the manufacturer's instructions (Promega). Luminescence and fluorescence were determined using a Synergy2 multifunction plate reader (Bio-Tek). pGudLuc luminescence was normalized to the CMV-green signal.

siRNA-mediated knockdown.

HepG2 cells were transfected with 50 nM siRNA targeting AHR (Origene, SR319302), HSPA9 (Qiagen FlexiTube GeneSolution GS3313, cat. No. GS3313), HSPA5 (Qiagen FlexiTube GeneSolution GS3309, cat. No. GS3309), HSP90AA1 (Qiagen FlexiTube GeneSolution GS3313, cat. No. SI00075971), TRAP1 (Qiagen FlexiTube GeneSolution, cat. No. SI00115150), HSPA1A (Qiagen FlexiTube GeneSolution GS3303, cat. No. GS3303), HSPB2 (Qiagen FlexiTube GeneSolution GS3316, cat. No. GS3316) or non-targeting scrambled siRNA (Santa Cruz Biotechnology, sc-37007). Briefly, a mix containing 25 pmol siRNA and 1 μl Lipofectamine 2000 was prepared in 100 μl of Opti-MEM (Thermo Fisher Scientific), incubated at room temperature for 20 min and then added to the cells. 48 h post transfection, cells were used for downstream applications (viral infection and plaque assay).

In silico PML Promoter analysis.

PML genomic sequence was obtained from NCBI. The DNA sequence of 1200 bp upstream of the protein coding regions was analyzed. P65/RelA and AHR binding sites were identified using Mulan.

Chromatin immunoprecipitation (ChIP).

HepG2 cells were mock-infected or infected with ZIKV. 48 h p.i. cells were prepared following ChIP-IT Express Enzymatic Shearing and ChIP protocol (#53009, Active Motif). Briefly, cells were fixed in 1%formaldehyde, washed in PBS and glycine Stop-Fix solution. Cells were pelleted, and chromatin was sheared using the Enzymatic Shearing Cocktail (Active Motif) for 10 min at 37°C. Shared chromatin as immunoprecipitated with 5 μg of antibody (anti-AHR, anti-NF-κB or control IgG) overnight at 4°C with rotation. The next day, magnetic beads were washed and cross-links were reversed in 0.1%SDS and 300 mM NaCl TE buffer at 63°C for 4 h. DNA fragments were purified using QIAquick PCR Purification Kit (#28104, QIAGEN). qPCR was performed using Fast SYBR Green Master Mix (#4385612, Thermo Fisher Scientific). The following primer pairs were used: AHR Binding site 1 forward, 5′-CGTAAGTCAGCGGTAGGTCTG -3′, and reverse, 5′-AGAGGCCGACTGTGGGTTTT -3′; AHR Binding site 2, 5′-CAGCTGTGGGCTCTCCTTTC -3′, and reverse, 5′-TACGGTAAAGCGGGAGAGGTA-3′; AHR Binding site 3 forward, 5′-TGACATGCTTTTCCATTGGCG -3′and reverse, 5′-AGCAGGATGATGCCTTGAGT-3′; AHR Binding site 4 forward, 5′-AGATGGCTGCCCACCATATTT-3′, and reverse, 5′-TGATAGGGCCTGGCTCTTGTA-3′; NFκB Binding site forward, 5′-CCCACCACCTACAACCCTAAA-3′, and reverse, 5′- CATTCTGGAAAGGAGAGCCC -3′

Measurement of Kyn and Trp concentrations by ELISA.

Kyn and Trp were quantified by ELISA (K3728 and K3730, ImmunDiagnostik) following manufacturer's instructions.

RNA-Sequencing.

RNA was extracted using the RNAeasy kit (Qiagen). 3' DGE RNA-Sequencing and library preparation were performed by The Broad Institute of Harvard and MIT. RNA-Seq libraries were prepared according to the single cell RNA-Seq libraries[55]. Reads were aligned using BWA Aln version 0.7.10 against the mm10/GRCm38 mouse reference and reads containing bases with quality lower than Q10 were removed. After alignment, reads were filtered out if it had more than one mismatch, more than 20As in a row (poly A tail), and aligned to more than 20 different positions in the transcriptome. Transcript quantifications were done using custom perl scripts and uniquely mapped reads with unique UMI's were processed for differential gene expression. Data analysis was performed using statistical software R version 3.3.3 and DESeq2 version 1.12.4. Differential genes were selected by ± 1.5-fold change. Heatmaps were generated using the GENE-E program and z-scores were calculated for each gene-row. GO terms were determined using Innate DB and Pathway analysis was done using the Ingenuity Pathway Analysis tool (https://www.qiagenbioinformatics.com/). To define upstream regulators, log2(Fold Change) values were assigned to each gene in each comparison. Upstream regulators were then predicted by IPA software (Qiagen).

To analyze the cell death pathway, 1 μg of total RNA was pooled from the brain tissue of 4 newborn mice from each group (NLP or NLP_{ANT}). Gene expression was analyzed using the RT^2 Profiler PCR Array Mouse Cell Death Pathway Finder (cat. no. PAMM-212ZA-Qiagen). Differential genes were selected by ± 2.0-fold change. Statistical analysis was performed using the RT2 profiler RT–PCR array data analysis software v3.5.

Nanoliposome construction.

Nanoliposomes were constructed using Sigma's Liposome kit (# L4395-5V) following the manufacturer's instructions. The nanoliposome preparations were serially extruded through a 200 nm and a 100 nm membrane and finally washed by ultracentrifugation. The nanoliposomes were resuspended in PBS and characterized before their use for their size (NLP 115.9±0.53, NLP_{ANT} 110.9±0.45), polydispersity index (NLP 0.066±0.003, NLP_{ANT} 0.082±0.003) and zeta potential (NLP 43±0.4, NLP_{ANT} 43.6±1.2).

In vivo ZIKV infection.

8–10 weeks old pregnant female SJL mice were intra-peritoneally infected with 10^6 PFUs of $ZIKV^{BR}$ (BeH815744) on E14 and followed daily. NLP_{ANT} were given daily from E13 until birth at 5 mg/kg bodyweight (total volume: 100 μl) also by i.p. route., receiving approximately 7 μg/animal of CH223191. HP163 was administered twice a day at 2.5 mg/kg bodyweight (total volume: 100 μl) by gavage. Crown-rump, biparietal, skull length, cranial height measurements were performed at E19 for HP163 and at the day of birth for NLPs. Neonates were measured using a pachymeter and weighted with a digital scale. All the experiments were performed with the approval of the Institute of Biomedical Sciences Ethics Committee – University of Sao Paulo.

Brain Histology.

Brains were removed from the skull and fixed in ice-cold 4% paraformaldehyde in 0.1 phosphate buffer pH 7.4 overnight, and cryoprotected in a solution of 30% sucrose in 0.1M phosphate buffer pH 7.4 at 4 °C. Samples were then frozen on dry ice, sectioned in the coronal plane at 20 μm thickness in a Leica semi-automatic cryostat (model 1850 UV, Leica Microsystems, Wetzlar, Germany) and mounted in super frost plus slides (VWR International, LLC Radnor, PA). Slides were dried for 48 hours, washed in distilled water for 2 minutes, incubated in Hematoxylin of Harris for 2 minutes, and then washed in running water to remove excess for 4 minutes. Slides were then incubated in Eosin for 2 minutes, dehydrated in increasing ethanol concentrations and diaphanization with xylol solution for 5 minutes and cover slipped with D.P.X. mounting medium (Sigma Aldrich, San Luis, MO, EUA). Images were acquired with an EVOS XL Core microscope (Thermo Fisher Scientific, MA, EUA) and analyzed by Image J Software.

Immunofluorescence.

Super frost plus mounted slides were blocked with blocking serum (3% donkey serum + 0,3% Triton X-100 in PBS) for 1 hour at room temperature. Sections were incubated with primary antibodies: Anti-pan flaviviruses Env (4G2) at 1:200 (anti-Rb GeneTex, Irvine, CA, USA); Anti-Nestin, 1:200 (anti-Gt, Santa Cruz Biotechnology, Dallas, TX, USA); and Anti-IBA1 (anti-Gt, Abcam, MA, USA) diluted in blocking serum, overnight at 4 °C. After incubation with the primary antibody, slides were incubated with secondary antibody (donkey anti-rabbit IgG, 488 and donkey anti-goat IgG, 594 Life technology, Carlsbad, CA, EUA; dilution 1:1000) diluted in PBS + 0,3% Triton X-100 for 2 hours at room temperature, protected from light. Slides were stained with DAPI for 20 minutes, 1:100.000 diluted in PBS + 0,3% Triton X-100 and coverslipped with Fluoromount G (Thermo Fisher, Waltham, MS, EUA) mounting medium. Images were acquired with a Nikon Eclipse 80i microscope (Nikon Instruments Inc., NY, USA) and analyzed by NIS- Elements Advanced Research 2.30 Image Software (Nikon Instruments Inc.).

Immunoblot analysis.

Cells were lysed with Cell Lysis buffer (1X) supplemented with protease inhibitor cocktail (Cell Signaling, USA). Total cell lysates (5–10 μg) were resolved on 4–12% Bis-Tris Nupage gels (Invitrogen, USA) and transferred onto PVDF membranes (Millipore) and developed with antibodies for GAPDH, NF-κB p65, Phospho-NF-κB p65, and anti-Rabbit IgG HRP-linked antibody using SuperSignal West Femto Maximum Sensitivity kit (Thermo Scientific), Data quantification was done using Image J software (NIH).

Alternatively, MOC1 and SUM149 cells were plated at 2 × 10 6 cells in T75 flasks and allowed to adhere overnight. Cells were pre-treated with 0.1% DMSO, 20 μM HP163 for 30 min and then treated with 0.1% DMSO, 100 μM Kyn or 1 nM TCDD for 1 hour. Nuclear and cytoplasmic cell extracts were prepared using a Nuclear Extract Kit (Thermo Scientific) as per the manufacturer's instructions. Protein concentration was quantified using the Protein Assay Reagent (Bio-Rad). Protein (30 μg) was resolved on 10% SDS-polyacrylamide gels and transferred to nitrocellulose membranes (Bio-Rad). Membranes were probed with mouse anti-AHR (Pierce, cat #MA1-514), rabbit anti-Lamin-A/C (Cell

Signaling, cat #2032) and mouse anti-α-tubulin (EMD Millipore, cat #CP06). Immunoreactive bands were detected using HRP-conjugated secondary antibodies (goat anti-rabbit, Bio-Rad; goat anti-mouse Pierce) and ECL substrate.

Statistical analysis.

GraphPad Prism software version 7 or 8 was used for statistical analysis. For *in vitro* studies, biological samples were randomly allocated into experimental groups at the beginning of the experiment. No statistical methods were used to predetermine sample size, but our sample sizes are similar to those reported in previous publications. For *in vivo* experiments, genetically identical animals were allocated randomly to experimental groups at the start of the experiments. No statistical methods were used to pre-determine sample sizes. Sample size was chosen based on previous experiments. Authors involved in data analysis were blinded to group assignment and data distribution was assumed to be normal, but this was not formally tested. Differences between groups were tested using a two-sided one sample t-test, a two-sided student's t-test, a one-way ANOVA followed by Tukey's post-hoc test (when testing every mean with every other mean) or a one-way ANOVA followed by Dunnet's post-hoc test (when comparing every mean to a control mean) as indicated in the figure legends for each experiment. A P value < 0.05 was considered significant.

Reporting summary.

Further information on research design is available in Life Sciences Reporting Summary attached to this article.

Data availability.

The authors declare that data supporting the findings of this study are available as Supplementary Tables 1–4. Sequencing data have been deposited into the Gene Expression Omnibus (GEO) under the SuperSeries accession numbers GSE147093 and GSE147094. Data from ZIKV-infected patients were accessed at GSE139181. Data from ZIKV-infected brain organoids were accessed at GSE129180.

Extended Data

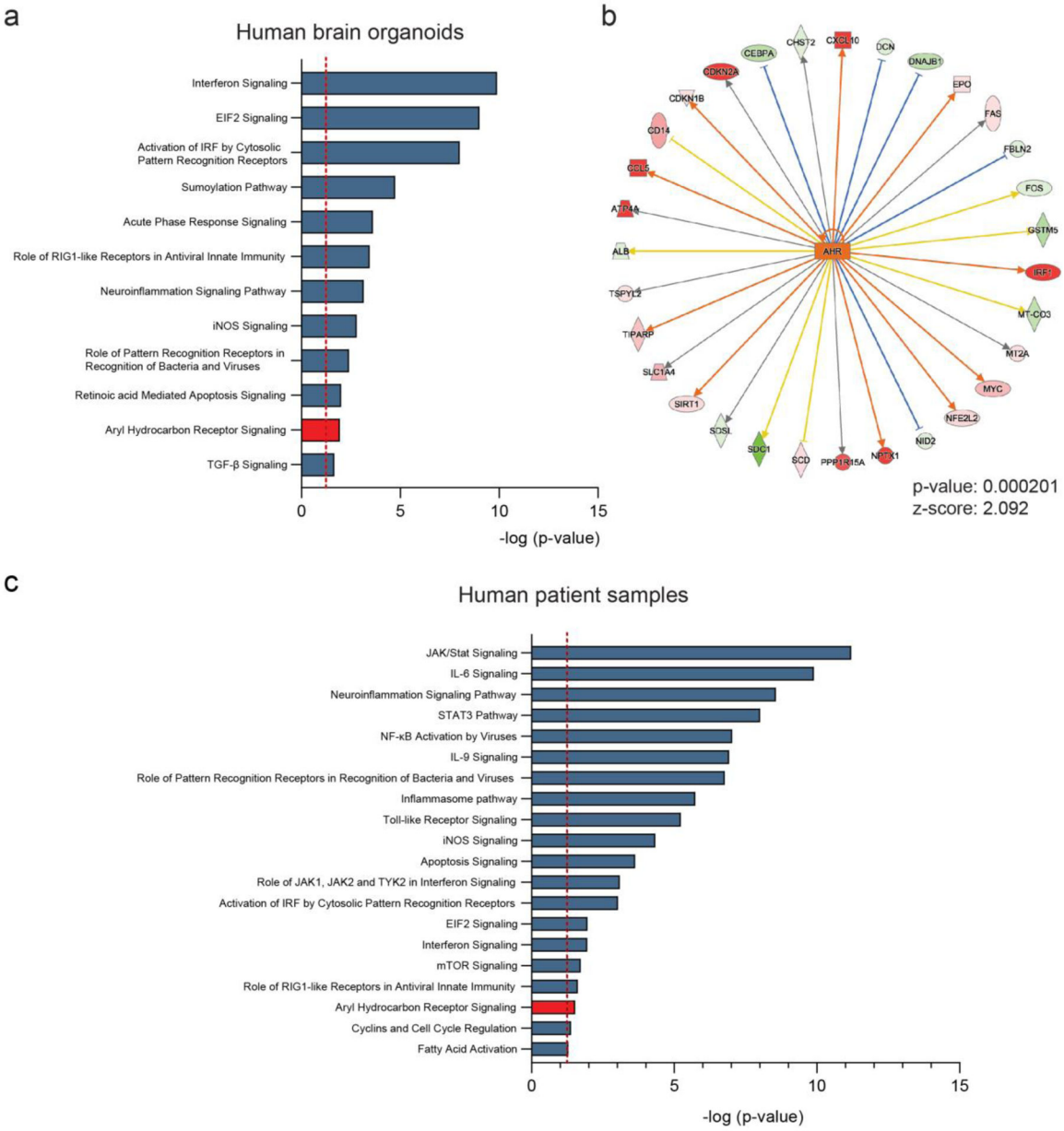

Extended Data Fig. 1.

(a) IPA analysis of RNA-seq data (GEO accession GSE129180) of ZIKV-infected human brain organoids. Pathways enriched in ZIKV-infected NPCs compared to control cells are shown (n=11 per condition). Dashed red line indicates p=0.05. p values were determined using Fisher's exact test (b) IPA analysis identified AHR as an upstream regulator. p values was determined using Fisher's exact test **(c)** IPA analysis of RNA-seq data (GEO accession GSE139181) of placental tissue from ZIKV-infected pregnant women compared to healthy controls (n=3 patients per condition). Pathways enriched in ZIKV-infection are shown. Dashed red line indicates p=0.05. p values were determined using Fisher's exact test.

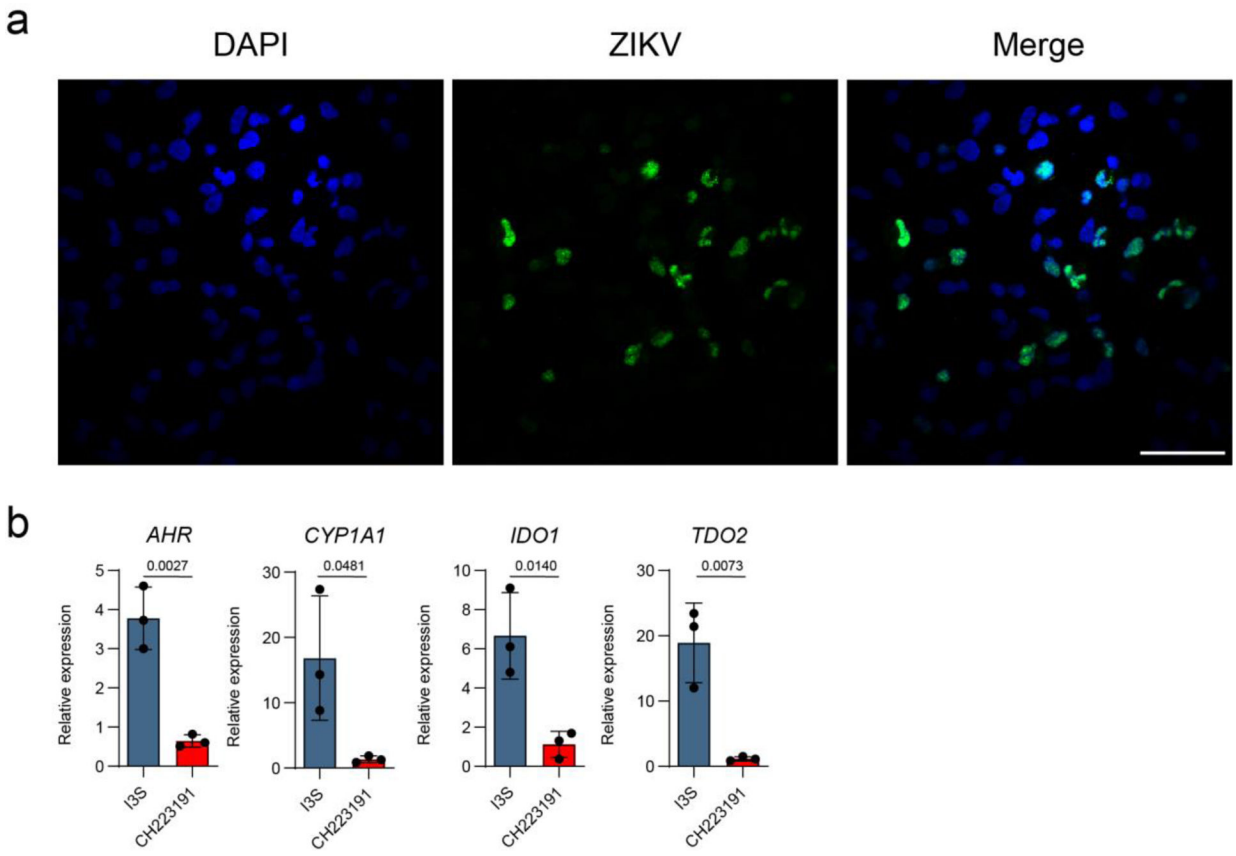

Extended Data Fig. 2.

(a) NPCs were infected with ZIKV (MOI = 1) and 48 h p.i., cells were fixed for immunofluorescence against ZIKV NS5 (green). Nuclei were counterstained with DAPI (blue). Images were acquired using an Olympus FV1000 confocal laser scanning microscope. Scale bar = 50 μm. Images are representative of 3 independent experiments. **(b)** *AHR* modulation in NPCs. NPCs were treated with I3S or a combination of I3S and CH223191. 24 h after treatment, NPCs were harvested for qPCR analysis of *AHR*, *CYP1A1*, *IDO1* and *TDO2*. Data represent the mean ± SD (n=3 independent experiments). p values were determined by a two-sided Student's t-test.

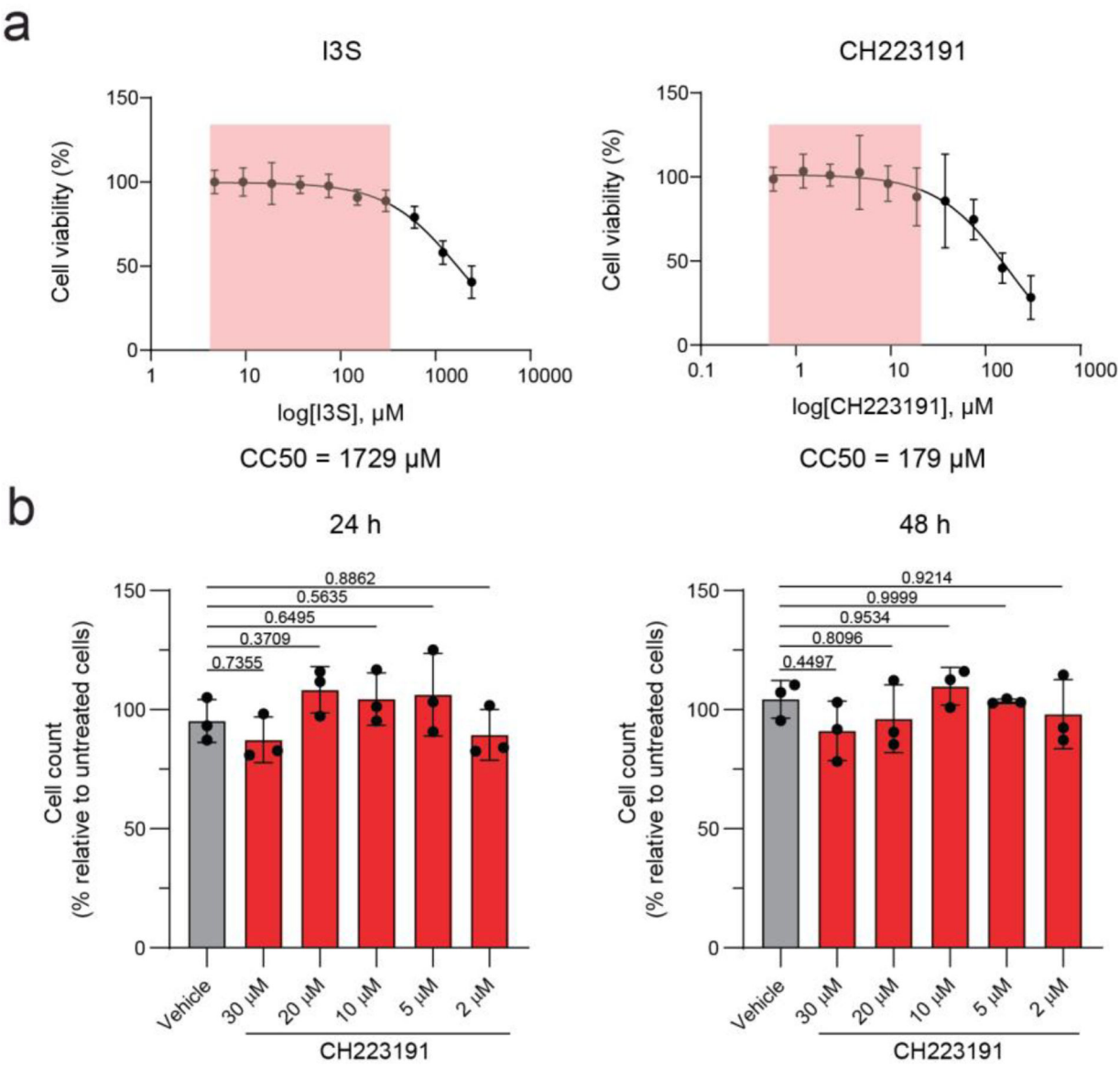

Extended Data Fig. 3.

(a) HepG2 cells viability after treatment for 24 h with different concentrations of I3S and CH223191 was evaluated by an MTT assay. Drug concentrations used for experiments are highlighted in color. Data represent the mean ± SD (n=3 independent experiments). **(b)** HepG2 cells were incubated for 24 h or 48 h with the indicated concentrations of CH223191 and the number of cells was quantified using a hemocytometer. Data represent the mean ± SD (n=3 independent experiments). p values were determined by a one-way ANOVA followed by Dunnet's post-hoc test.

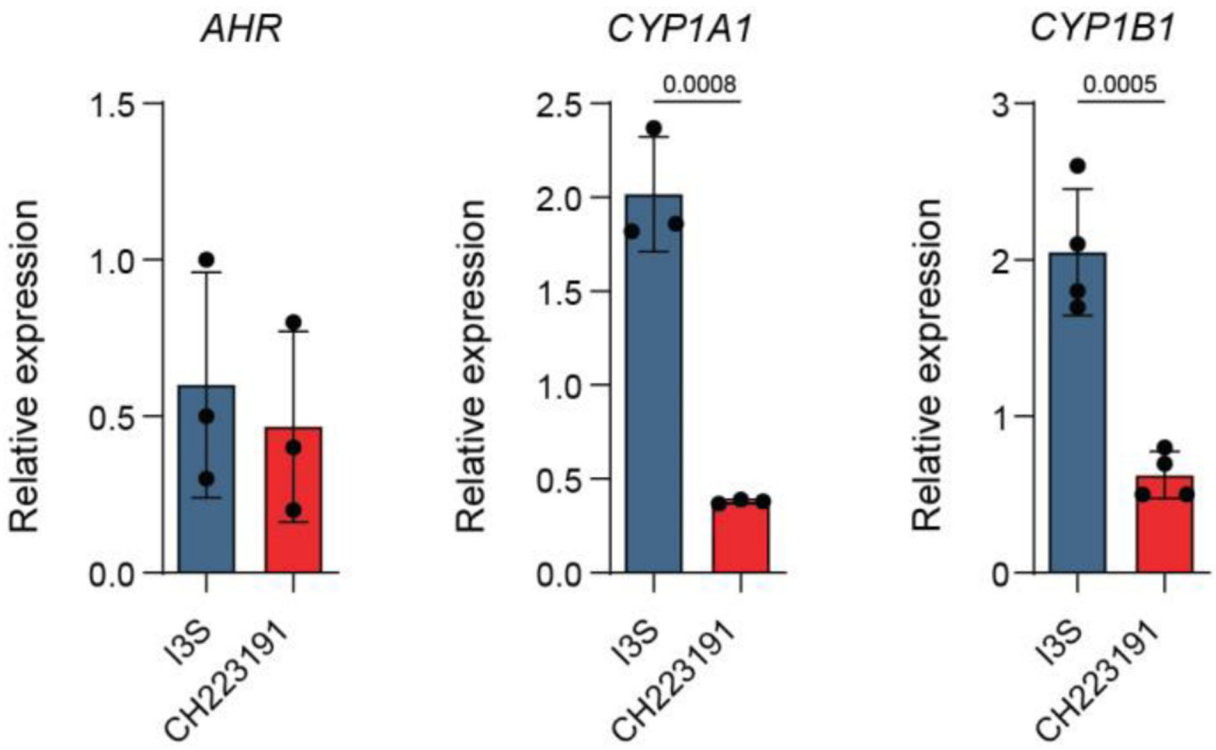

Extended Data Fig. 4.

Vero cells were treated with I3S or a combination of I3S and CH223191. 48 h after treatment, cells were harvested for qPCR analysis of *AHR*, *CYP1A1*, and *CYP1B1*. Data represent the mean ± SD (n=3 independent experiments for *AHR*, *CYP1A1*; n=4 for *CYP1B1*). p values were determined by a two-sided Student's t-test.

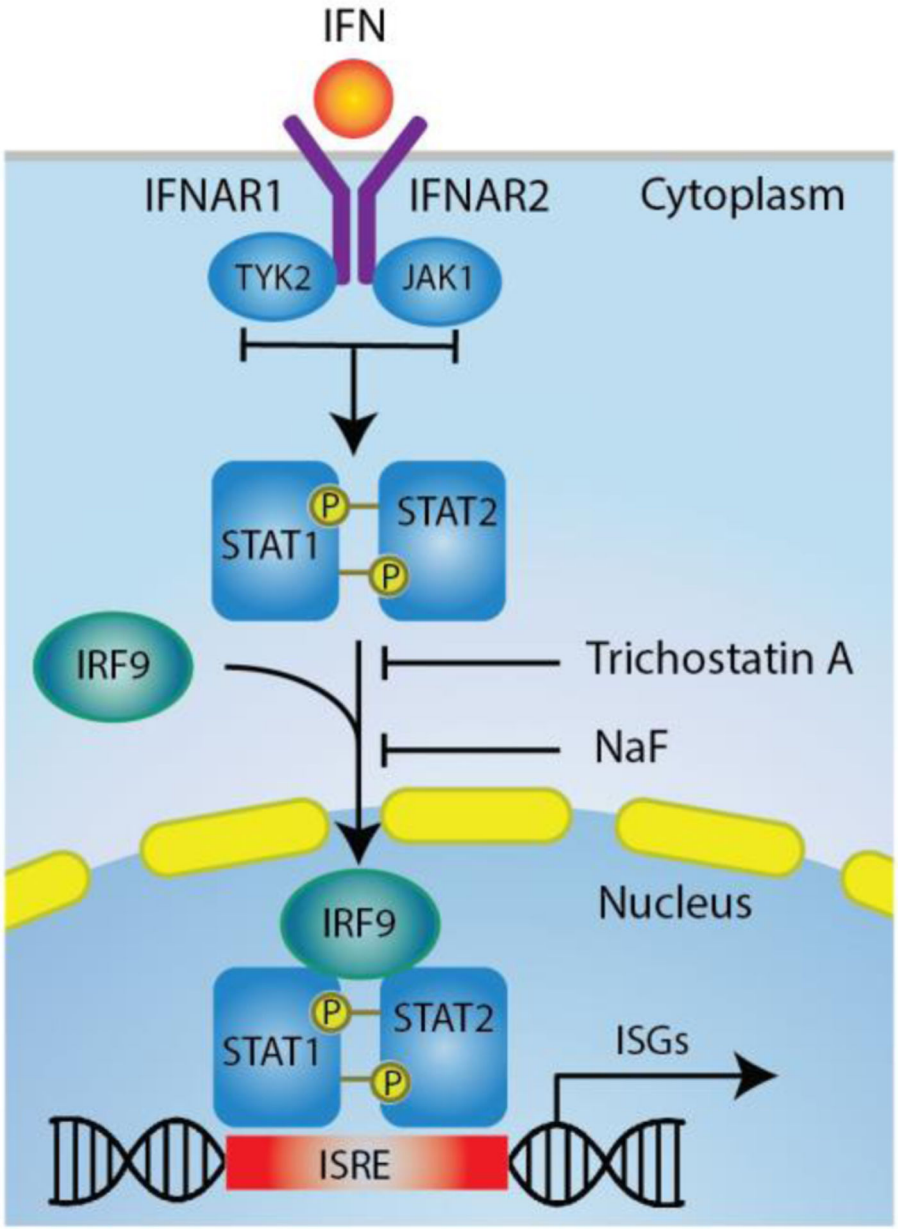

Extended Data Fig. 5.

Schematic representation of the IFN-I pathway. Trichostatin A inhibits the assembly of STAT1/STAT2/IRF9 complex and NaF impairs its translocation to the nucleus.

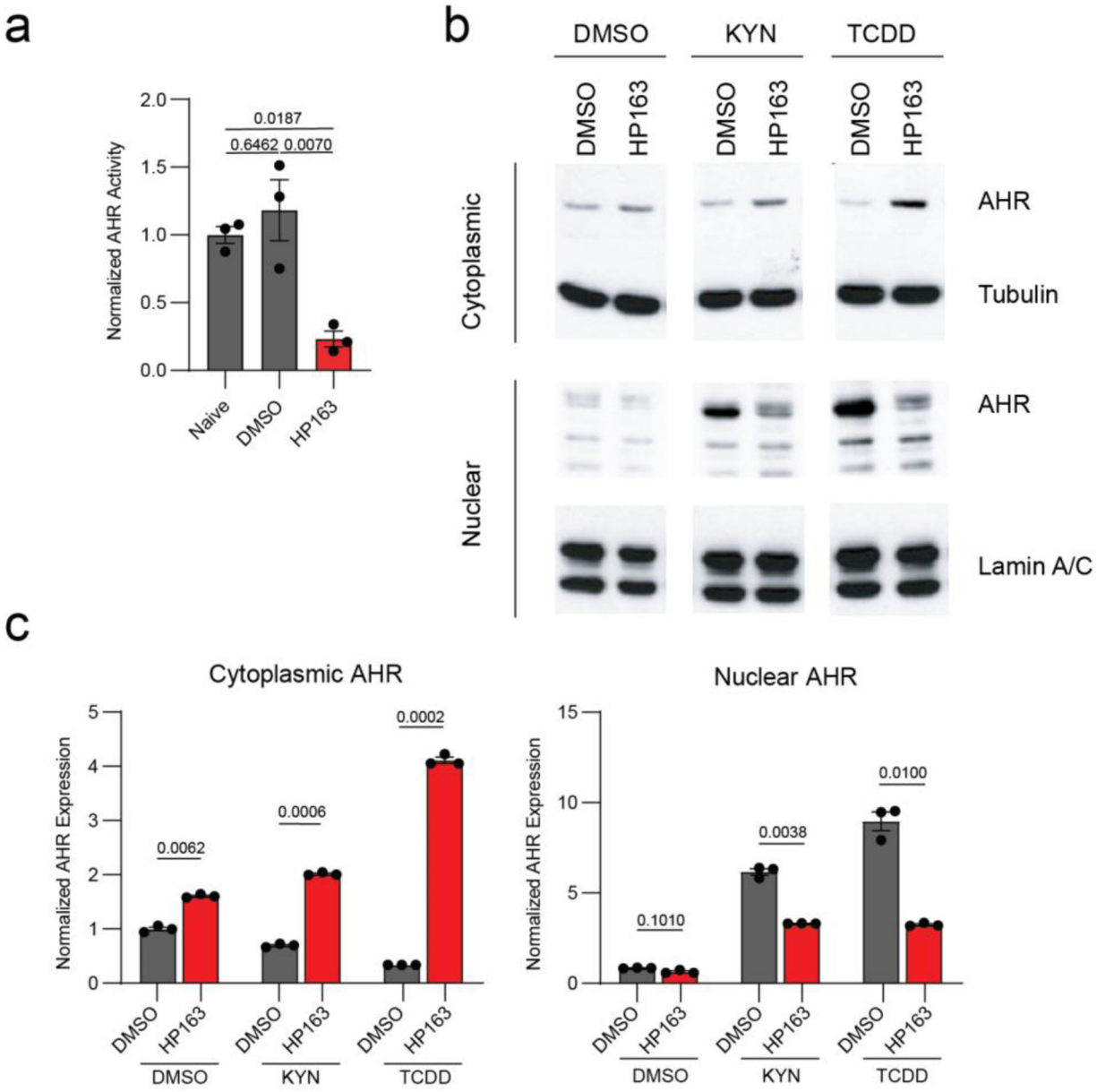

Extended Data Fig. 6.

(a) SUM149 cells were transfected with the AHR-driven pGudLuc reporter construct and treated with DMSO (vehicle) or 20 μM HP163. Twenty-four hours later cells were assayed for pGudLuc (luciferase) activity and normalized to the CMV-green fluorescence signal. Data represent the mean ± SD (n=3 independent experiments). p values were determined by a one-way ANOVA followed by Tukey's post-hoc test **(b)** Murine MOC1 oral cancer cells were treated with DMSO (vehicle) or 20 μM HP163 for 30 min and then treated with DMSO, 100 μM Kyn or 1 nM TCDD. Nuclear and cytoplasmic extracts were prepared and AHR protein quantified by Western immunoblotting. White spaces between gel pieces indicates cropping of the original image. Data are representative of three independent experiments. **(c)** Quantification of Western immunoblotting bands from the three

experiments described in (b). Data are presented as mean ± SD (n=3 independent experiments). p values were determined by a two-sided Student's t-test.

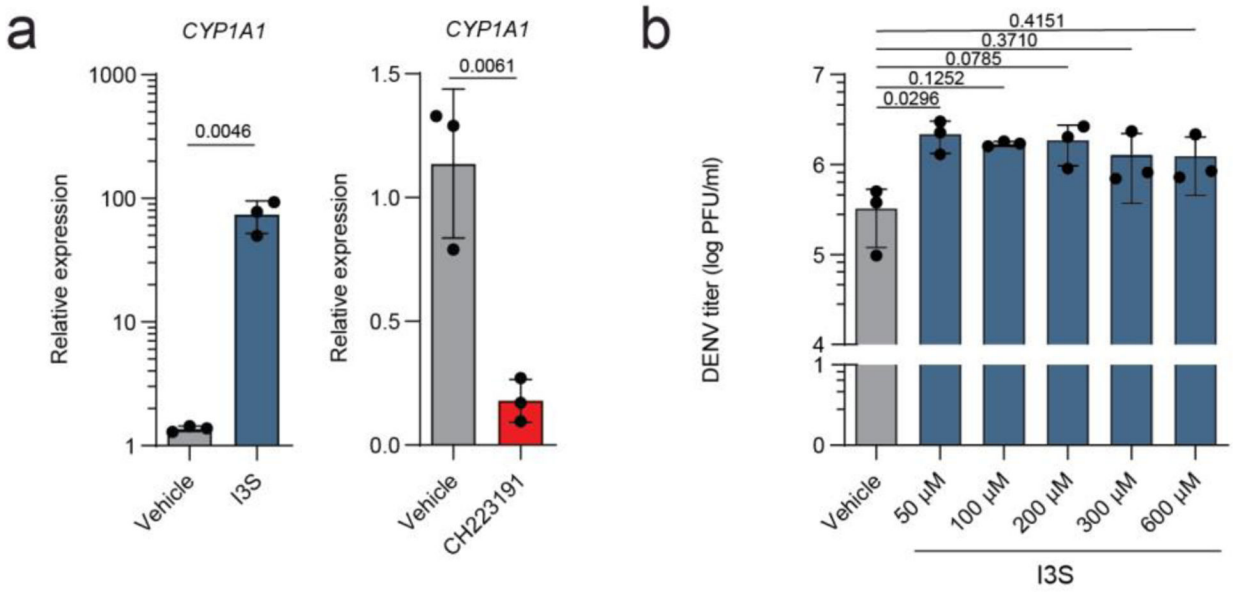

Extended Data Fig. 7.

(a) A549 cells were treated with I3S (50 μM) or CH223191 (2 μM) for 24 h. Then, cells were harvested for qPCR analysis of *CYP1A1*. Data represent the mean ± SD (n=3 independent experiments). p values were determined by a two-sided Student's t-test. **(b)** AHR activation boosts DENV replication. A549 cells were pretreated with the indicated concentrations of I3S for 24 h and infected with DENV-2 (MOI = 0.1). 48 h p.i. supernatants were harvested for plaque assay. Data represent the mean ± SD (n=3 independent experiments). p values were determined by a one-way ANOVA followed by Dunnet's post-hoc test.

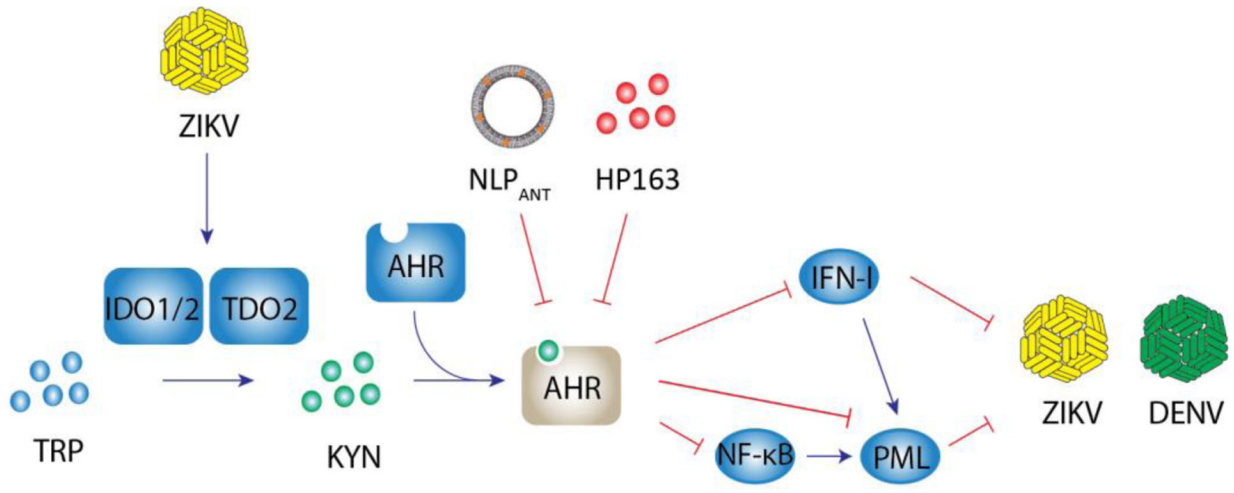

Extended Data Fig. 8.

IDO1/TDO2 upregulation induced by ZIKV infection boosts the generation of Kyn, which activates AHR to inhibit IFN-I dependent and IFN-I independent mechanisms that limit ZIKV replication as follows: 1) AHR activation limits IFN-I. 2) AHR also limits NF-kB activation, suppressing PML expression. AHR signaling may also operate in a similar manner to promote DENV replication.

Supplementary Material

Refer to Web version on PubMed Central for supplementary material.

Acknowledgments:

This work was supported by grants NS102807, NS087867, ES02530, AI126880, AI093903 and AI100190 from the National Institutes of Health, USA; RSG-14-198-01-LIB from the American Cancer Society and RG4111A1 and JF2161-A-5 from the National Multiple Sclerosis Society to FJQ. FJQ received support from the International Progressive MS Alliance. C.C.G. was supported by Universidad de Buenos Aires (UBA) (20020160100091BA), Consejo Nacional de Investigaciones Científicas y Tecnológicas (CONICET) (PIP11220170100171CO) and Agencia de Promoción Científica y Tecnológica (ANPCyT) (BID-PICT 3080). C.C.G is member of the Research Career CONICET. F.G. was supported by a Du Pre grant from the International MS Foundation and a post-doctoral fellowship from CONICET. J.P.S.P was supported by FAPESP (2017/26170-0 and 2017/22504-1). C.M.P and N.G.Z received a FAPESP fellowship (2017/11828-0 and 2016/07371-2). We thank all members of the Garcia and Quintana laboratories for helpful advice and discussions.

References

1. Baud D, Gubler DJ, Schaub B, Lanteri MC & Musso D An update on Zika virus infection. The Lancet 390, 2099–2109 (2017).
2. Musso D & Gubler DJ Zika Virus. Clinical Microbiology Reviews 29, 487–524 (2016). [PubMed: 27029595]
3. Faria NR, et al. Establishment and cryptic transmission of Zika virus in Brazil and the Americas. Nature 546, 406–410 (2017). [PubMed: 28538727]
4. França GVA, et al. Congenital Zika virus syndrome in Brazil: a case series of the first 1501 livebirths with complete investigation. The Lancet 388, 891–897 (2016).
5. Cao-Lormeau VM, et al. Guillain-Barre Syndrome outbreak associated with Zika virus infection in French Polynesia: a case-control study. Lancet 387, 1531–1539 (2016). [PubMed: 26948433]
6. Boldescu V, Behnam MAM, Vasilakis N & Klein CD Broad-spectrum agents for flaviviral infections: dengue, Zika and beyond. Nature Reviews Drug Discovery 16, 565–586 (2017). [PubMed: 28473729]
7. Yan N & Chen ZJ Intrinsic antiviral immunity. Nature Immunology 13, 214–222 (2012). [PubMed: 22344284]
8. Perelygin AA, et al. Positional cloning of the murine flavivirus resistance gene. Proceedings of the National Academy of Sciences 99, 9322–9327 (2002).
9. Giovannoni F, et al. Dengue Non-structural Protein 5 Polymerase Complexes With Promyelocytic Leukemia Protein (PML) Isoforms III and IV to Disrupt PML-Nuclear Bodies in Infected Cells. Frontiers in Cellular and Infection Microbiology 9 (2019).
10. Macnamara FN Zika virus: a report on three cases of human infection during an epidemic of jaundice in Nigeria. Trans R Soc Trop Med Hyg 48, 139–145 (1954). [PubMed: 13157159]
11. Liang Q, et al. Zika Virus NS4A and NS4B Proteins Deregulate Akt-mTOR Signaling in Human Fetal Neural Stem Cells to Inhibit Neurogenesis and Induce Autophagy. Cell Stem Cell 19, 663–671 (2016). [PubMed: 27524440]
12. Tang H, et al. Zika Virus Infects Human Cortical Neural Progenitors and Attenuates Their Growth. Cell Stem Cell 18, 587–590 (2016). [PubMed: 26952870]

13. Liu L, et al. Protection of ZIKV infection-induced neuropathy by abrogation of acute antiviral response in human neural progenitors. Cell death and differentiation 26, 2607–2621 (2019). [PubMed: 30952992]
14. Lum FM, et al. Immunological observations and transcriptomic analysis of trimester-specific full-term placentas from three Zika virus-infected women. Clinical & translational immunology 8, e01082 (2019). [PubMed: 31709049]
15. Gutierrez-Vazquez C & Quintana FJ Regulation of the Immune Response by the Aryl Hydrocarbon Receptor. Immunity 48, 19–33 (2018). [PubMed: 29343438]
16. Opitz CA, et al. An endogenous tumour-promoting ligand of the human aryl hydrocarbon receptor. Nature 478, 197–203 (2011). [PubMed: 21976023]
17. Cugola FR, et al. The Brazilian Zika virus strain causes birth defects in experimental models. Nature 534, 267–271 (2016). [PubMed: 27279226]
18. Rothhammer V & Quintana FJ The aryl hydrocarbon receptor: an environmental sensor integrating immune responses in health and disease. Nature reviews. Immunology 19, 184–197 (2019).
19. Rothhammer V, et al. Microglial control of astrocytes in response to microbial metabolites. Nature 557, 724–728 (2018). [PubMed: 29769726]
20. Rothhammer V, et al. Type I interferons and microbial metabolites of tryptophan modulate astrocyte activity and central nervous system inflammation via the aryl hydrocarbon receptor. Nat Med 22, 586–597 (2016). [PubMed: 27158906]
21. Yamaguchi M & Hankinson O 2,3,7,8Tetrachlorodibenzopdioxin suppresses the growth of human liver cancer HepG2 cells in vitro: Involvement of cell signaling factors. Int J Oncol 53, 1657–1666 (2018). [PubMed: 30066859]
22. Choi EY, Lee H, Dingle RW, Kim KB & Swanson HI Development of novel CH223191-based antagonists of the aryl hydrocarbon receptor. Mol Pharmacol 81, 3–11 (2012). [PubMed: 21967751]
23. Richardson RB, et al. A CRISPR screen identifies IFI6 as an ER-resident interferon effector that blocks flavivirus replication. Nature microbiology 3, 1214–1223 (2018).
24. Elong Ngono A & Shresta S Immune Response to Dengue and Zika. Annual Review of Immunology 36, 279–308 (2018).
25. Pfeffer LM, et al. Role of Nuclear Factor-κB in the Antiviral Action of Interferon and Interferon-regulated Gene Expression. Journal of Biological Chemistry 279, 31304–31311 (2004).
26. Luecke S, Wincent E, Backlund M, Rannug U & Rannug A Cytochrome P450 1A1 gene regulation by UVB involves crosstalk between the aryl hydrocarbon receptor and nuclear factor kappaB. Chemico-biological interactions 184, 466–473 (2010). [PubMed: 20132803]
27. Yamada T, et al. Constitutive aryl hydrocarbon receptor signaling constrains type I interferon–mediated antiviral innate defense. Nature Immunology 17, 687–694 (2016). [PubMed: 27089381]
28. Dixit E, et al. Peroxisomes Are Signaling Platforms for Antiviral Innate Immunity. Cell 141, 668–681 (2010). [PubMed: 20451243]
29. Franz KM, Neidermyer WJ, Tan Y-J, Whelan SPJ & Kagan JC STING-dependent translation inhibition restricts RNA virus replication. Proceedings of the National Academy of Sciences 115, E2058–E2067 (2018).
30. Hubackova S, Krejcikova K, Bartek J & Hodny Z Interleukin 6 Signaling Regulates Promyelocytic Leukemia Protein Gene Expression in Human Normal and Cancer Cells. Journal of Biological Chemistry 287, 26702–26714 (2012).
31. Stanford EA, et al. The role of the aryl hydrocarbon receptor in the development of cells with the molecular and functional characteristics of cancer stem-like cells. BMC Biol 14, 20 (2016). [PubMed: 26984638]
32. Taguwa S, et al. Defining Hsp70 Subnetworks in Dengue Virus Replication Reveals Key Vulnerability in Flavivirus Infection. Cell 163, 1108–1123 (2015). [PubMed: 26582131]
33. Brass AL, et al. The IFITM Proteins Mediate Cellular Resistance to Influenza A H1N1 Virus, West Nile Virus, and Dengue Virus. Cell 139, 1243–1254 (2009). [PubMed: 20064371]
34. Zhang R, et al. A CRISPR screen defines a signal peptide processing pathway required by flaviviruses. Nature 535, 164–168 (2016). [PubMed: 27383988]

35. Marceau CD, et al. Genetic dissection of Flaviviridae host factors through genome-scale CRISPR screens. Nature 535, 159–163 (2016). [PubMed: 27383987]
36. Zhou Q, Lavorgna A, Bowman M, Hiscott J & Harhaj EW Aryl Hydrocarbon Receptor Interacting Protein Targets IRF7 to Suppress Antiviral Signaling and the Induction of Type I Interferon. Journal of Biological Chemistry 290, 14729–14739 (2015).
37. Nganou-Makamdop K, et al. Type I IFN signaling blockade by a PASylated antagonist during chronic SIV infection suppresses specific inflammatory pathways but does not alter T cell activation or virus replication. PLoS pathogens 14, e1007246 (2018). [PubMed: 30142226]
38. Gagliani N, et al. Th17 cells transdifferentiate into regulatory T cells during resolution of inflammation. Nature 523, 221–225 (2015). [PubMed: 25924064]
39. Takenaka MC, et al. Control of tumor-associated macrophages and T cells in glioblastoma via AHR and CD39. Nature neuroscience 22, 729–740 (2019). [PubMed: 30962630]
40. Schiering C, et al. Feedback control of AHR signalling regulates intestinal immunity. Nature 542, 242–245 (2017). [PubMed: 28146477]
41. Yockey LJ, et al. Type I interferons instigate fetal demise after Zika virus infection. Science immunology 3 (2018).
42. Hernandez-Ochoa I, Karman BN & Flaws JA The role of the aryl hydrocarbon receptor in the female reproductive system. Biochemical pharmacology 77, 547–559 (2009). [PubMed: 18977336]
43. Lawrence BP & Vorderstrasse BA New insights into the aryl hydrocarbon receptor as a modulator of host responses to infection. Seminars in Immunopathology 35, 615–626 (2013). [PubMed: 23963494]
44. Wheeler JLH, Martin KC & Lawrence BP Novel Cellular Targets of AhR Underlie Alterations in Neutrophilic Inflammation and Inducible Nitric Oxide Synthase Expression during Influenza Virus Infection. The Journal of Immunology 190, 659–668 (2012). [PubMed: 23233726]
45. Winans B, et al. Linking the Aryl Hydrocarbon Receptor with Altered DNA Methylation Patterns and Developmentally Induced Aberrant Antiviral CD8+T Cell Responses. The Journal of Immunology 194, 4446–4457 (2015). [PubMed: 25810390]
46. Safe S, Cheng Y & Jin UH The Aryl Hydrocarbon Receptor (AhR) as a Drug Target for Cancer Chemotherapy. Curr Opin Toxicol 2, 24–29 (2017). [PubMed: 28459113]
47. Geoffroy M-C & Chelbi-Alix MK Role of Promyelocytic Leukemia Protein in Host Antiviral Defense. Journal of Interferon & Cytokine Research 31, 145–158 (2011). [PubMed: 21198351]
48. Franchini AM & Lawrence BP Environmental exposures are hidden modifiers of anti-viral immunity. Current Opinion in Toxicology 10, 54–59 (2018). [PubMed: 30035244]
49. Thackray LB, et al. Oral Antibiotic Treatment of Mice Exacerbates the Disease Severity of Multiple Flavivirus Infections. Cell Reports 22, 3440–3453.e3446 (2018). [PubMed: 29590614]
50. Manfredo Vieira S, et al. Translocation of a gut pathobiont drives autoimmunity in mice and humans. Science 359, 1156–1161 (2018). [PubMed: 29590047]
51. Judd NP, et al. ERK1/2 regulation of CD44 modulates oral cancer aggressiveness. Cancer research 72, 365–374 (2012). [PubMed: 22086849]
52. Bosch I, et al. Rapid antigen tests for dengue virus serotypes and Zika virus in patient serum. Sci Transl Med 9 (2017).
53. Chan JF, et al. Improved detection of Zika virus RNA in human and animal specimens by a novel, highly sensitive and specific real-time RT-PCR assay targeting the 5'-untranslated region of Zika virus. Trop Med Int Health 22, 594–603 (2017). [PubMed: 28214373]
54. Lanciotti RS, et al. Genetic and serologic properties of Zika virus associated with an epidemic, Yap State, Micronesia, 2007. Emerg Infect Dis 14, 1232–1239 (2008). [PubMed: 18680646]
55. Soumillon M, Cacchiarelli D, Semrau S, van Oudenaarden A & Mikkelsen TS Characterization of directed differentiation by high-throughput single-cell RNA-Seq. (Cold Spring Harbor Laboratory, 2014).

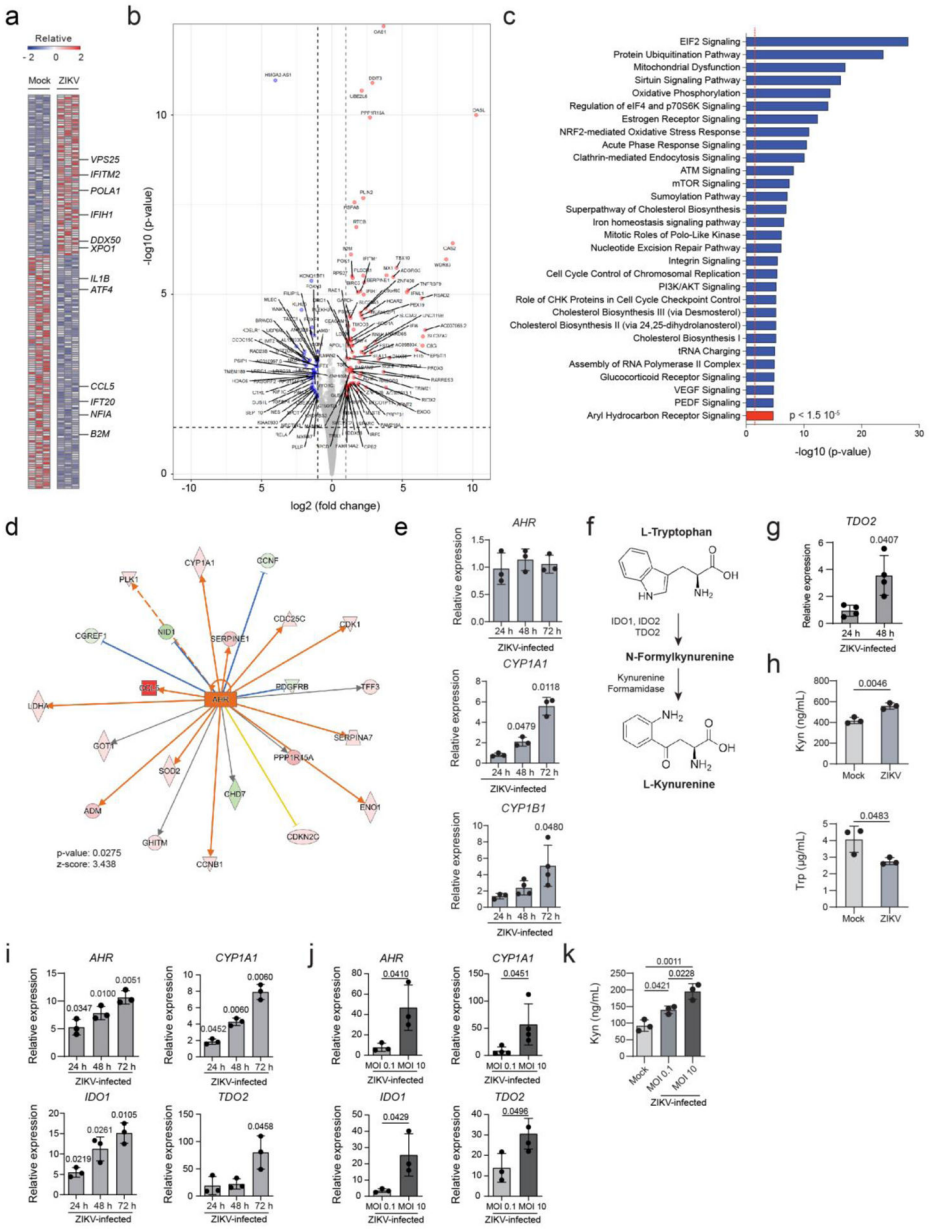

Figure 1: AHR signaling is activated by ZIKV infection *in vitro*.

(a) Differentially expressed genes between mock-infected and ZIKV-infected HepG2 cells identified by RNA-Seq (n=3 independent experiments per condition). **(b)** Volcano plot highlighting differentially expressed genes in samples from (a) Colors code for up- and down-regulation of individual members in red and blue, respectively. p values were determined by a Wald test and adjusted for multiple comparisons using the Benjamini–Hochberg correction. (**c**) Ingenuity pathway analysis (IPA) of pathways enriched in ZIKV-infected HepG2 cells compared to mock-infected cells (n=3 independent experiments per condition). Dashed red line indicates p=0.05. p values were determined using a Fisher's exact test **(d)**. IPA identified AHR as an upstream regulator. p value was determined using a Fisher's exact test (**e**) mRNA expression determined by qPCR at different timepoints of

ZIKV infection of HepG2 cells (MOI = 1). Expression values are relative to mock-infected cells. Data are mean ± SD (n=3 independent experiments for *AHR* and *CYP1A1*; n=4 for *CYP1B1*). p values were determined by a two-sided one-sample t-test. **(f)** Schematic representation of the Kyn pathway. **(g)** *TDO2* expression determined by qPCR in ZIKV-infected HepG2 cells (MOI = 1). Expression values are relative to mock-infected cells. Data represent the mean ± SD (n=4 independent experiments). p values were determined by a two-sided one-sample t-test. **(h)** ELISA quantification of Trp and Kyn in culture supernatants 48 h p.i. after infection of HepG2 cells with ZIKV (MOI = 1). Data represent the mean ± SD (n=3 independent experiments). p values were determined by a two-sided Student's t-test. **(i)** mRNA expression determined by qPCR in ZIKV-infected NPCs (MOI = 1). Expression values are relative to mock-infected cells. Data are mean ± SD (n=3 independent experiments). p values were determined using a two-sided one-sample t-test. **(j)** Effect of MOI on mRNA expression in ZIKV-infected NPCs 48 h p.i. Expression values are relative to mock-infected cells. Data are mean ± SD. (n=3 independent experiments for *AHR*, *IDO1*, *TDO2*; n=4 for *CYP1A1*). p values were determined by a two-sided Student's t-test. **(k)** ELISA quantification of Kyn in supernatants of ZIKV-infected NPCs 48 h p.i. Data represent the mean ± SD (n=3 independent experiments). p values were determined by a one-way ANOVA followed by Tukey's post-hoc test.

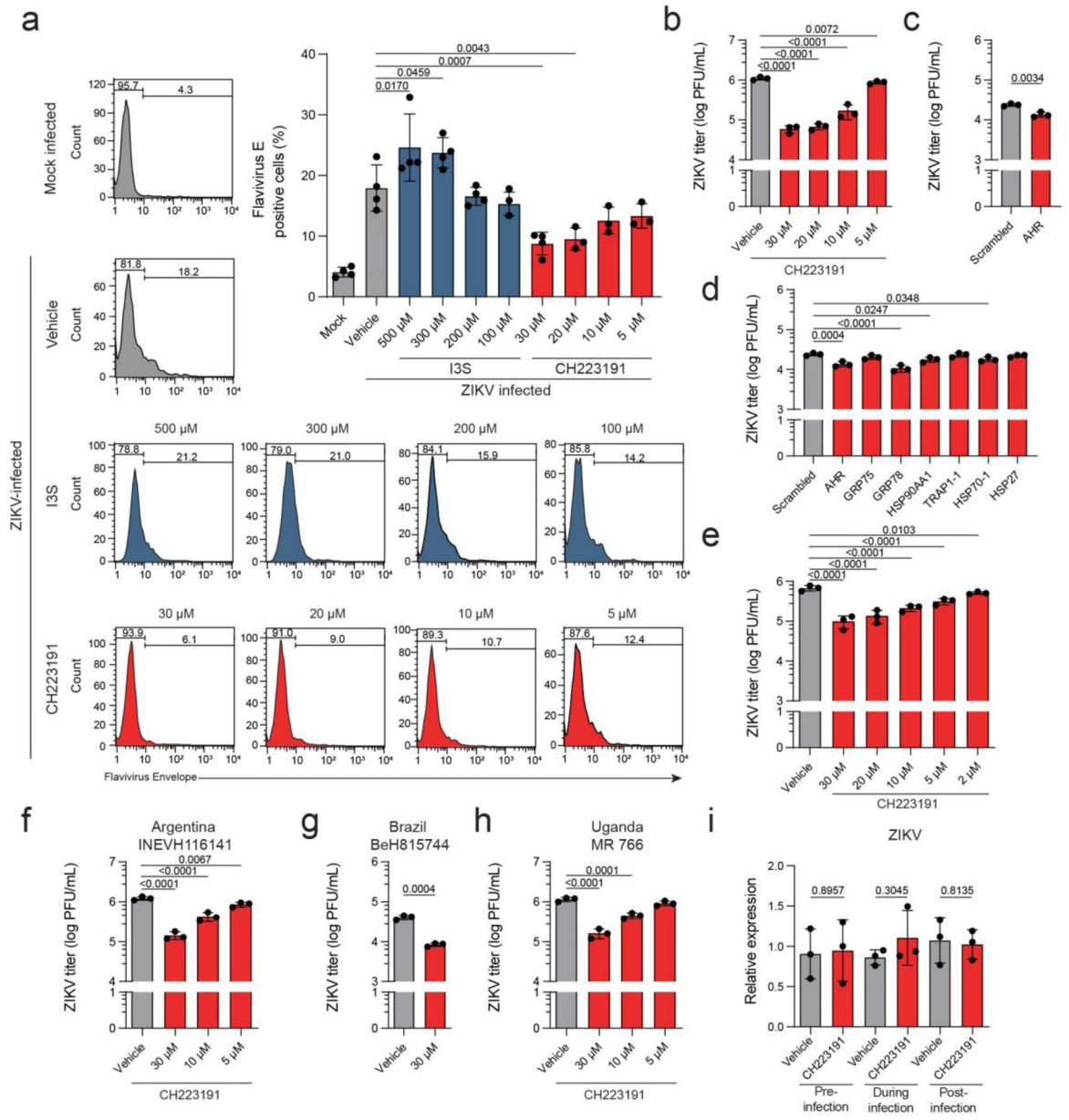

Figure 2: AHR signaling boosts ZIKV replication *in vitro*.

(**a**) Flow cytometry quantification of HepG2 cells positive for flavivirus antigen. HepG2 cells were pre-treated with different concentrations of I3S, CH223191 or DMSO (vehicle) and infected with ZIKV (MOI = 1) for 48 h. Plots shown are representative of one experiment. Bar graphs represent the mean ± SD of flavivirus antigen positive cells (n=4 independent experiments for samples mock, vehicle, I3S 500-200 µM and CH223191 30 µM or n=3 for samples I3S 100 µM, CH223191 20- 5 µM). p values were determined by a one-way ANOVA followed by Dunnett's post-hoc test. (**b,e**) Quantification by plaque assay of infectious virus particles in the supernatants of HepG2 cells (b), and human NPCs (e) pre-treated with CH2213191 or DMSO (vehicle) . Data represent the mean ± SD (n=3 independent experiments). p values were determined by a one-way ANOVA followed by

Dunnett's post-hoc test. **(c,d)** Quantification of infectious virus particles in AHR knock down or control HepG2 cells. HepG2 cells were transfected with scrambled-siRNA or AHR-siRNA (c), infected with ZIKV (MOI = 0.1) and 48 h p.i. supernatants were harvested for plaque assay. The same experiment was performed using other relevant siRNAs indicated in the figure (d). Data represent the mean ± SD (n=3 independent experiments). p values were determined by a two-sided Student's t-test (c) or a one-way ANOVA followed by Dunnett's post-hoc test (d). (**f-h**) Quantification by plaque assay of infectious virus particles in the supernatants of HepG2 cells pre-treated with CH223191 or DMSO (vehicle) 48 h after infection with ZIKV INEVH116141 (Argentina) (f) BeH815744 (Brazil) (g), and MR 766 (Uganda) (h). Data represent the mean ± SD (n=3 independent experiments). p values were determined by a two-sided Student's t-test (g) or one-way ANOVA followed by Dunnett'spost-hoc test (f,h). **(i)** qPCR quantification of ZIKV RNA in HepG2 cells treated with CH223191 or DMSO (vehicle) pre-infection, during adsorption or internalization of ZIKV (MOI = 3). 2 h p.i., cells were harvested for qPCR to determine the level of ZIKV RNA. Data represent the mean ± SD (n=3 independent experiments). p values were determined by a two-sided Student's t-test.

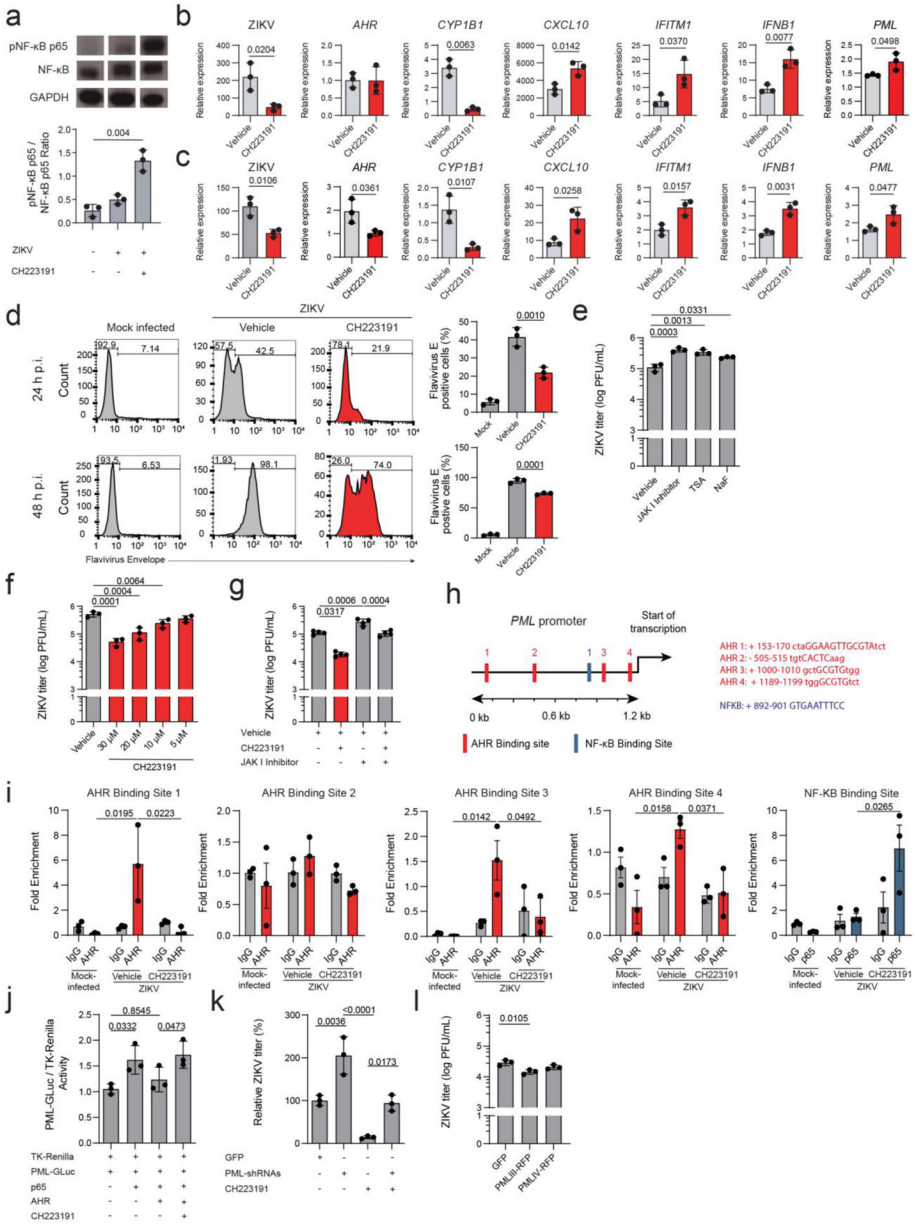

Figure 3: AHR limits IFN-I dependent and PML-driven intrinsic immunity to ZIKV.

(**a**) NF-κB activation in ZIKV-infected and CH223191-treated cells determined by Western Blot. HepG2 cells were pre-treated with CH223191,infected with ZIKV and harvested for WB analysis. White spaces between gel pieces indicates cropping of the original image. Data represent the mean ± SD (n=3 independent experiments). p values were determined by a one-way ANOVA followed by Tukey's post-hoc test. (**b,c**) mRNA and viral RNA levels determined by qPCR in ZIKV-infected HepG2 cells (b) or human NPCs (c) pre-treated with CH223191 or DMSO (vehicle). Expression of cellular genes shown are relative to non-treated, mock-infected cells. RNA level of ZIKV is relative to ZIKV-infected cells immediately harvested after infection. Data represent the mean ± SD (n=3 independent experiments). p values were determined by a two-sided Student's t-test **(d)** Flow cytometry

quantification of Vero cells expressing flavivirus antigen. Vero cells were pre-treated with CH223191 or DMSO (vehicle) and infected with ZIKV (MOI = 1). Flow cytometry plots are representative of one experiment. Bar graphs shown on the right represent the mean ± SD of virus antigen positive cells (n=3 independent experiments). p values were determined by a one-way ANOVA followed by Dunnet's post-hoc test. **(e)** Effect of inhibitors of IFN signaling on ZIKV replication determined 24 h p.i. by plaque assay. HepG2 cells were pre-treated with DMSO (vehicle), JAK 1 Inhibitor, TSA, or NaF and infected with ZIKV. Data represent the mean ± SD (n=3 independent experiments). p values were determined by a one-way ANOVA followed by Dunnett's post-hoc test. (**f**) Quantification of infectious virus particles in supernatants of Vero cells pre-treated with CH223191 or DMSO (vehicle) and infected with ZIKV (MOI =1). 48 h p.i. supernatants were harvested for plaque assay. Data represent the mean ± SD (n=3 independent experiments). p values were determined by a one-way ANOVA followed by Dunnett's post-hoc test. (**g**) Effect of CH223191 on HepG2 cells treated with JAK I inhibitor. HepG2 cells were treated with JAK 1 Inhibitor and CH223191 as indicated in the figure, infected with ZIKV (MOI = 0.1), and 24 h p.i. supernatants were harvested for plaque assay . Data represent the mean ± SD (n=4 independent experiments). p values were determined by a one-way ANOVA followed by Tukey's post-hoc test. (**h**) Schematic representation of the *PML* promoter. Predicted binding sites to AHR and NF-κB were determined using Mulan software. **(i)** ChIP analysis of AHR and NF-κB binding sites in the *PML* promoter. HepG2 cells were treated with CH223191 or DMSO (vehicle) and infected with ZIKV as indicated in the figure. 48 h p.i. ChIP was performed using AHR and NF-κB-specific antibodies or non-specific IgG. Data are mean ± SD (n=3 independent experiments). p values were determined by a one-way ANOVA followed by Tukey's post-hoc test. **(j)** Luciferase assay using a construct coding for the *PML* promoter cloned upstream of the reporter gene *Gaussia* Luciferase. HEK-293 cells were pre-treated with CH223191 and transfected with plasmids as indicated. 24 h post transfection, cells were harvested for Luciferase quantification. Data represent the mean ± SD (n=3 independent experiments). p values were determined by a one-way ANOVA followed by Tukey's post-hoc test. (**k**) HeLa cells were transfected with a plasmid encoding for GFP (control) or PML-shRNAs and pre-treated with CH223191 as indicated in the figure.Then, cells were infected with ZIKV (MOI = 1) and 24 h p.i. supernatants were harvested for quantification of infectious virus particles by plaque assay. Viral titers were normalized to non-transfected cells. Data represent the mean ± SD (n=3 independent experiments). p values were determined by a one-way ANOVA followed by Tukey's post-hoc test. (**l**) Effect of PMLIII and PMLIV on ZIKV production. HepG2 cells were transfected with plasmids encoding for GFP (control), PMLIII-RFP or PMLIV-RFP, infected with ZIKV (MOI = 0.1) and 24 h p.i., supernatants were harvested for quantification of infectious virus particles by plaque assay. Data represent the mean ± SD (n=3 independent experiments). p values determined by a one-way ANOVA followed by Dunnet's post-hoc test.

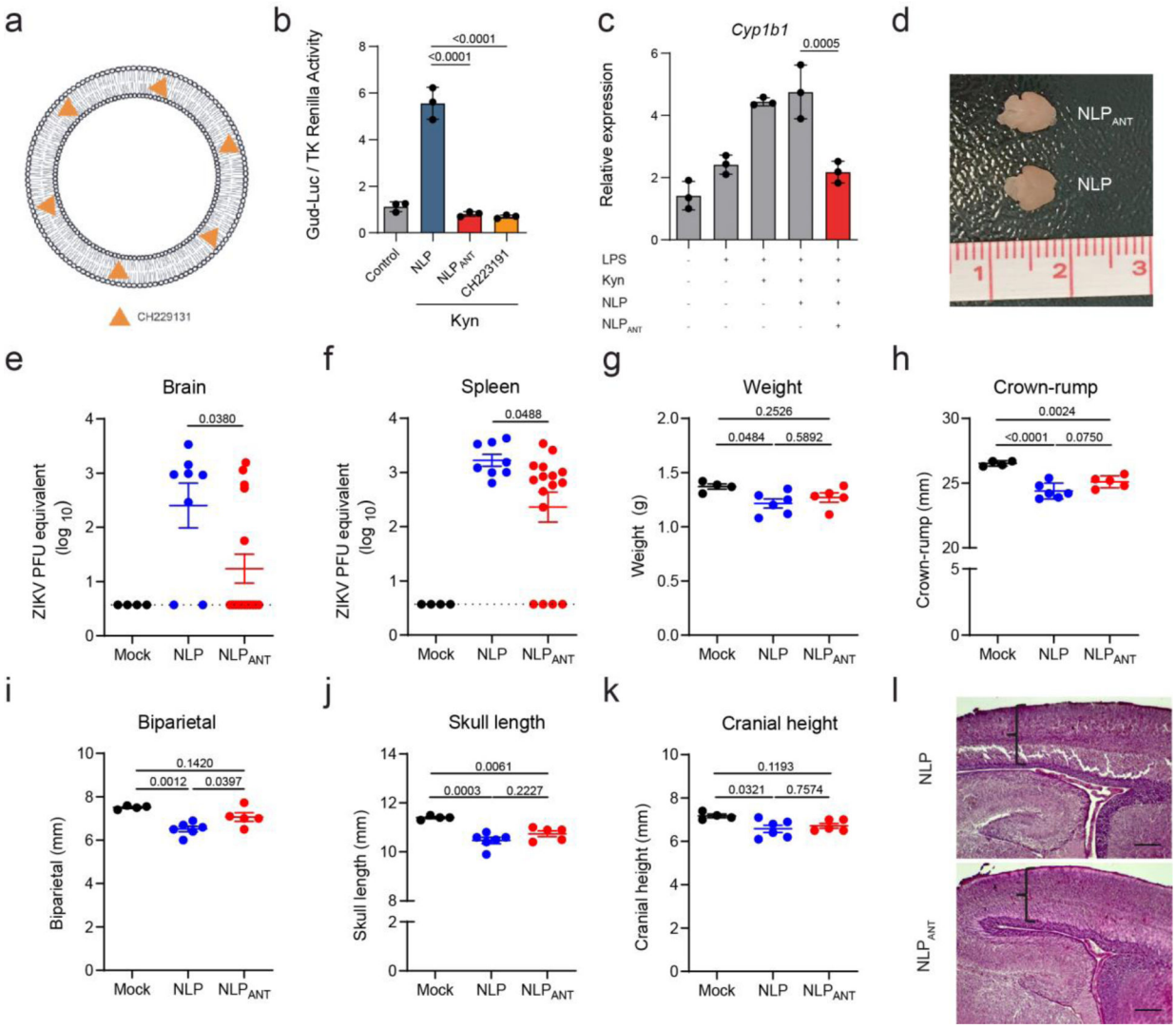

Figure 4: Nanoliposome-delivered AHR antagonist limits ZIKV replication and microcephaly *in vivo*.

(a) Schematic representation of nanoliposomes loaded with CH223191. **(b)** HEK-293 cells were transfected with an AHR-responsive reporter (pGud-Luc) and treated as indicated with Kyn, NLP, NLP_{ANT} or CH223191. Data represent the mean ± SD (n=3 independent experiments). p values were determined by a one-way ANOVA followed by Tukey's post-hoc test. **(c)** Bone marrow-derived DCs were treated with Kyn and NLP, NLP_{ANT} or CH223191 and the expression of *Cyp1b1* was determined by qPCR. Data represent the mean ± SD (n=3 independent experiments). p values were determined by a one-way ANOVA followed by Tukey's post-hoc test. **(d)** Pictures of pups' brains from ZIKV-infected pregnant SJL mice treated with NLP or NLP_{ANT} . Image is representative of 3 animals that showed similar results**(e-f)** ZIKV viral load in brain and spleen of pups from ZIKV-infected pregnant SJL mice treated with NLP, NLP_{ANT} or from non-infected controls. Data represent the mean ± SD (n=8 pups from NLP-treated mothers, n=16 pups from NLP_{ANT}-treated mothers and n=4 pups from non-infected mothers). p values were determined by a one-way ANOVA followed by Tukey's post-hoc test. **(g-k)** Macroscopic analyses of pups at birth. All pups

were evaluated at birth for weight and skull measurements (crown-rump, biparietal, skull length, and cranial height). Data represent the mean ± SD (n=6 pups from NLP-treated mothers, n=5 pups from NLP_{ANT}-treated mothers and n=4 pups from mock-infected mothers).. p values were determined by a one-way ANOVA followed by Tukey's post-hoc test **(l)** Brain histology of hippocampal region of pups from ZIKV-infected mothers treated with NLP or NLP_{ANT}. Brackets indicate cortical thickness. Scale bar = 200 μm. Image shown is representative of 3 animals that showed similar results.

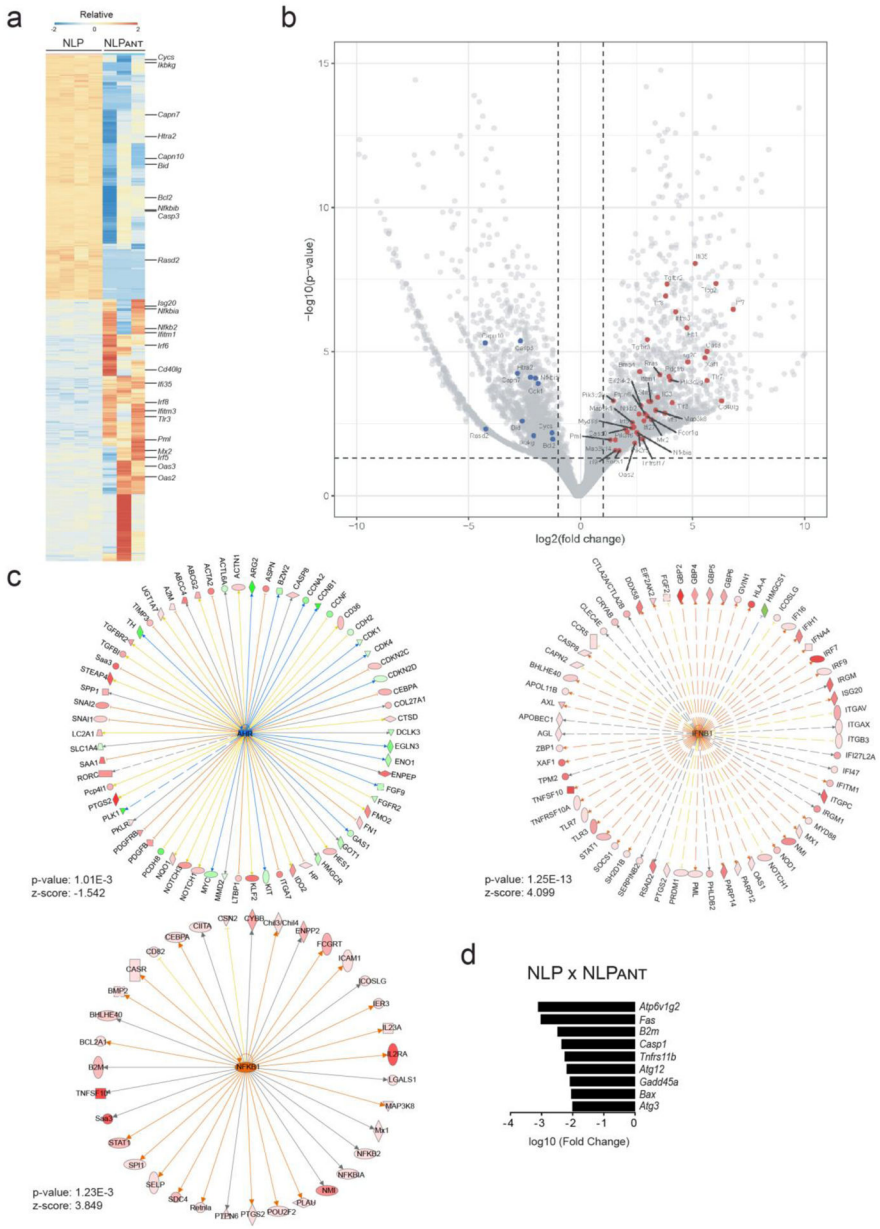

Figure 5. Transcriptional effects of AHR antagonism during ZIKV infection *in vivo*.

(a) RNA-Seq analysis of CNS fetal samples from NLP- or NLP_{ANT}-treated ZIKV infected mice (n=4 or n=3 pups respectively). **(b)** Volcano plot highlighting differentially expressed genes in samples from (a). Colors code for up- and down-regulation of individual members in red (up) and blue (down), respectively. p values were determined by a Wald test and adjusted for multiple comparisons using the Benjamini–Hochberg correction **(c)** . IPA identified AHR, IFNB1 and NFKB1 as upstream regulators. p values were determined using a Fisher's exact test **(d)** Cell death gene expression transcriptional signature. Pooled brain RNA from 3 pups from NLP and NLP_{ANT} treated mothers were used for PCR array analysis for Cell Death Pathway Finder RT^2 Profiler . Data are expressed as fold change comparing the two groups.

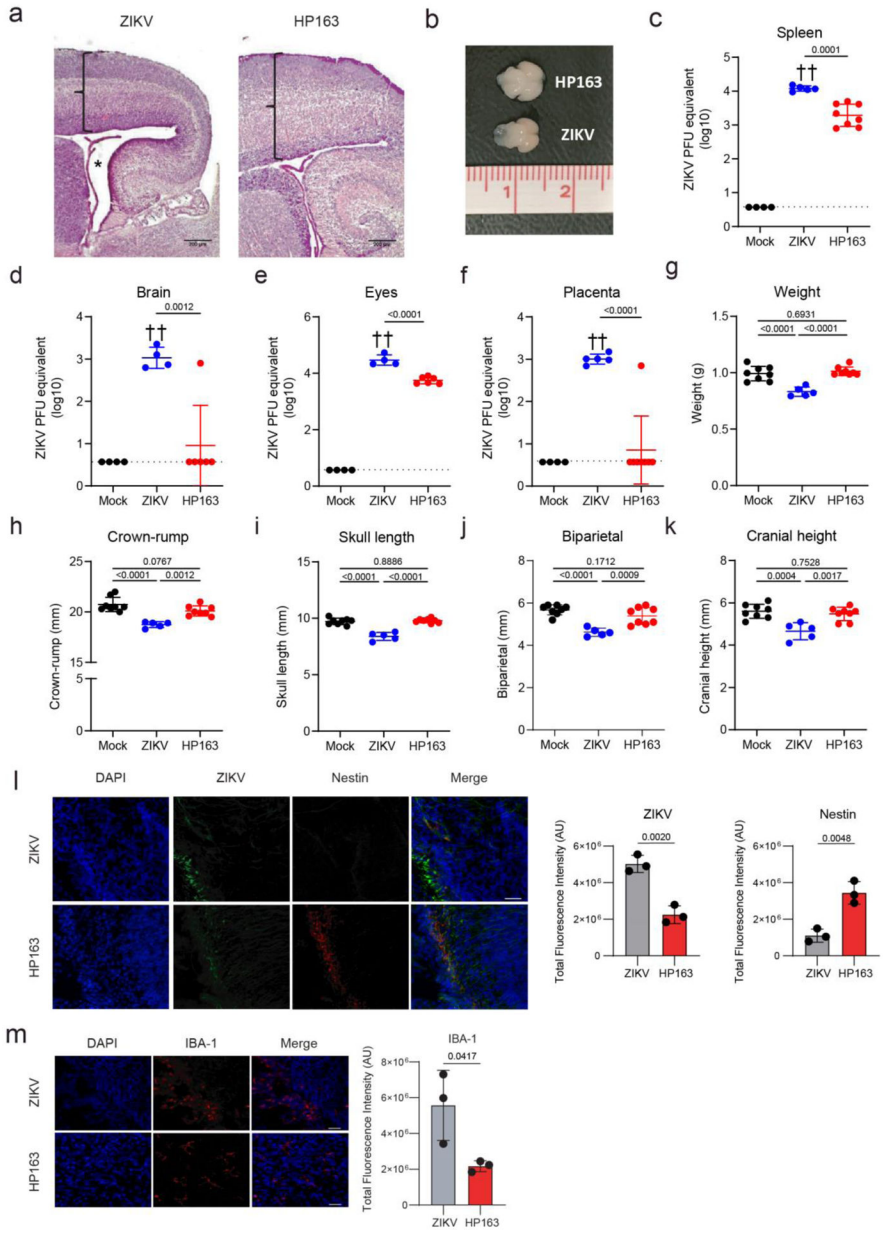

Figure 6: A novel oral AHR antagonist limits ZIKV replication and microcephaly *in vivo*.

(a) Histological analysis of fetal hippocampus and cortex from vehicle and HP163-treated ZIKV-infected mothers. Asterisks indicate ventricle dilatation and brackets indicate cortical thickness. Scale bar = 200 μm. Image is representative of 2 animals that showed similar results. **(b)** Brains from pups used in (a). Image is representative of 2 animals that showed similar results. **(c-f)** ZIKV viral load in spleen, brain, eyes from pups, and placenta from infected pregnant SJL mice treated with HP163 or vehicle. Data represent the mean ± SD (n=4 pups from mock-infected mothers, n=5 pups from ZIKV-infected mothers and n=8 pups from ZIKV-infected HP163-treated mothers in (c) and (f) or n=4 pups from mock-infected mothers, n=4 pups from ZIKV-infected mothers and n=6 pups from ZIKV-infected HP163-treated mothers in (d) an (e)). p values were determined by a one-way ANOVA

followed by Tukey's post-hoc test. † indicate fetal death. **(g-k)** Macroscopic evaluation of pups at birth. Data represent the mean ± SD (n=8 pups from mock-infected mothers, n=5 pups from ZIKV-infected mothers, n=8 pups from ZIKV-infected HP163-treated mothers) p values were determined by a one-way ANOVA followed by Tukey's post-hoc test. **(l)** Immunofluorescence of fetal brains from SJL mothers infected with ZIKV and treated with HP163 or vehicle. Staining against nestin and ZIKV was performed using specific antibodies. Nuclei were counterstained with DAPI and imaging was performed using a standard fluorescence microscope. Scale bar = 500 μm. Data represent the mean ± SD (n=3 independent samples). p values were determined by a two-sided Student's t-test. **(m)** Immunofluorescence using specific antibodies against IBA-1 was performed as in (l). Scale bar = 500 μm. Data represent the mean ± SD (n=3 independent samples). p values were determined by a two-sided Student's t-test.

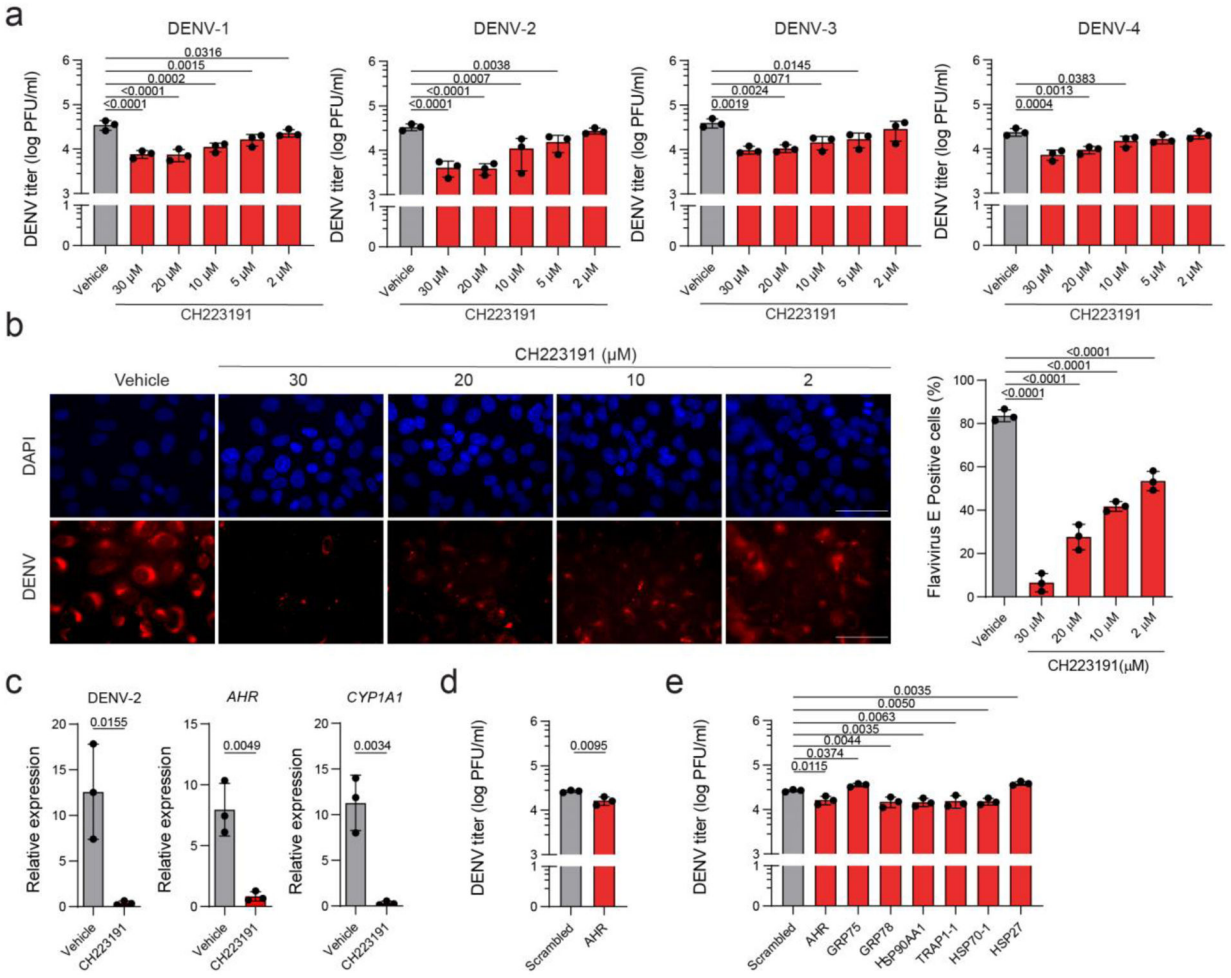

Figure 7: AHR modulation affects DENV replication

(a) Infectious virus particles in the supernatants of A549 cells pre-treated with CH2213191 and infected with DENV-1, DENV-2, DENV-3 or DENV-4 (MOI = 0.1). At 24 h p.i. supernatants were harvested for plaque assay. Data represent the mean ± SD (n=3 independent experiments). p values were determined by a one-way ANOVA followed by Dunnet's post-hoc test. **(b)** A549 cells positive for flavivirus antigen determined by immunofluorescence. Cells infected with DENV-2 from (a) were stained against flavivirus envelope protein and visualized under a fluorescence microscope. Images of random fields of view were acquired and the number of cells positive for flavivirus antigen was counted using FIJI. Scale bar = 40 μm. Data represent the mean ± SD (n=3 independent experiments). p values were determined by a one-way ANOVA followed by Dunnet's post-hoc test. **(c)** mRNA and viral RNA levels determined by qPCR in DENV-2-infected cells. A549 cells were infected with DENV-2 (MOI = 0.1) and 48 h p.i. they were harvested for qPCR analysis. Data represent the mean ± SD (n=3 independent experiments). p values were determined by a two-sided Student's t-test **(d,e)** Infectious virus particles in supernatants of A549 cells transfected with scrambled-siRNA, AHR-siRNA (d) or other relevant siRNAs indicated in the figure (e). Cells were transfected, infected with DENV-2 (MOI = 0.1) and 48 h p.i. supernatants were harvested for plaque assay. Data represent the mean ± SD (n=3

independent experiments). p values were determined by a two-sided Student's t-test (d) or one-way ANOVA followed by Dunnet's post-hoc test (e).